Precipitates and intermetallic phases in precipitation hardening Al–Cu–Mg–(Li) based alloys

S. C. Wang*[1,2] and M. J. Starink[1]

The present study contains a critical review of work on the formation of precipitates and intermetallic phases in dilute precipitation hardening Al–Cu–Mg based alloys with and without Li additions. Although many suggestions for the existence of pre-precipitates in Al–Cu–Mg alloys with a Cu/Mg atomic ratio close to 1 have been made, a critical review reveals that evidence exists for only two truly distinct ones. The precipitation sequence is best represented as: supersaturated solid solution→co-clusters→GPB2/S"→S where clusters are predominantly Cu–Mg co-clusters (also termed GPB or GPB I zones), GPB2/S" is an orthorhombic phase that is coherent with the matrix (probable composition $Al_{10}Cu_3Mg_3$) for which both the term GPB2 and S" have been used, and S phase is the equilibrium Al_2CuMg phase. GPB2/S" can co-exist with S phase before the completion of the formation of S phase. It is further mostly accepted that the crystal structure of S' (Al_2CuMg) is identical to the equilibrium S phase (Al_2CuMg). The Perlitz and Westgren model for S phase is viewed to be the most accepted structure. 3DAP analysis showed that Cu–Mg clusters form within a short time of natural and artificial aging. Cu–Mg clusters and S phase contribute to the first and second stage hardening during aging. In Al–Cu alloys, the θ phase (Al_2Cu) has I4/mcm structure with a=0·607 nm and c=0·487 nm, and θ' phase with tetragonal structure and a=0·404 nm, c=0·58 nm, the space group is $I\bar{4}m2$. Gerold's model for θ" (or GPII) appears to be favourable in terms of free energy, and is consistent with most experimental data. The transformation from GPI to GPII (or θ") seems continuous, and as Cu atoms will not tend to cluster together or cluster with vacancies, the precipitation sequence can thus be captured as: supersaturated solid solution→θ" (Al_3Cu)→θ' (Al_2Cu)→θ (Al_2Cu). The Ω phase (Al_2Cu) has been variously proposed as monoclinic, orthorhombic, hexagonal and tetragonal distorted θ phase structures. It has been shown that Ω phase forms initially on $\{111\}_{Al}$ with c=0·935 nm and on further aging, the c lattice parameter changes continuously to 0·848 nm, to become identical to the orthorhombic structure proposed by Knowles and Stobbs (a=0·496 nm, b=0·858 nm and c=0·848 nm). Other models are either wrong (for example, monoclinic and hexagonal) or refer to a transition phase (for example, the Garg and Howe model with c=0·858 in a converted orthorhombic structure). For Al–Li–Cu–Mg alloys, the $L1_2$ ordered metastable δ' (Al_3Li) phase has been observed by many researchers. The Huang and Ardell model for T_1 phase (space group P6/mmm, a=0·496 nm and c=0·935 nm), appears more likely than other proposed structures. Other proposed structures are perhaps due to the T_1 phase forming by the dissociation of $\frac{1}{2}\langle 110\rangle$ dislocations into $1/6\langle 211\rangle$ Shockley partials bounding a region of intrinsic stacking fault, in which copper and lithium enrichment of the fault produces a thin layer of the T_1 phase.

Keywords: Precipitates, Precipitation hardening, Crystal structures, Al–Cu–Mg alloys

[1]Materials Research Group, School of Engineering Sciences, The University of Southampton, Southampton SO17 1BJ, UK
[2]Electron Microscopy Centre, Faculty of Engineering and Science, The University of Southampton, Southampton SO17 1BJ, UK

*Corresponding author, email wangs@soton.ac.uk

Introduction

The phenomenon of precipitation hardening was first discovered in an Al–4Cu–0·6Mg (wt-%) alloy by the German chemist Alfred Wilm in 1906. This alloy is

Published by Maney for the Institute and ASM International
DOI 10.1179/174328005X14357

International Materials Reviews IMR413.3d 22/4/05 21:23:12
The Charlesworth Group, Wakefield +44(0)1924 369598 - Rev 7.51n/W (Jan 20 2003)

S.C. Wang and M.J. Starink, Review of precipitation in Al-Cu-Mg(-Li) alloys, Int Mater Rev., 2005, Vol. 50, pp 193-215

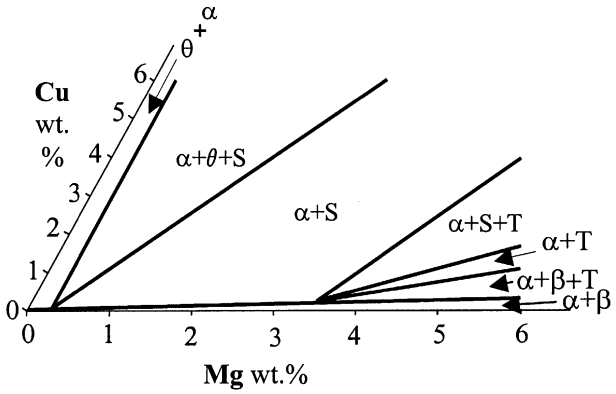

1 Isothermal section of ternary Al–Cu–Mg phase diagram at 200°C; α=Al, θ=$CuAl_2$, S=Al_2CuMg, T=Al_6CuMg_4 and β=$Al_{12}Mg_{17}$ (adapted from Ref. 1)

situated in the $\alpha+\theta+S$ phase field of the Al–Cu–Mg phase diagram (Fig. 1).[1] Since this discovery, a wide range of heat treatable aluminium alloys have been developed, and alloys based on Al–Cu and Al–Cu–Mg compositions are today an important class, collectively known as the 2xxx class of aluminium alloys. Table 1 shows the nominal compositions of some commercial Al–Cu–Mg–(Li) alloys.[2,3] One of the major alloys is 2024 [Al–4·2Cu–1·5Mg–0·6Mn (wt-%)], which was introduced in the 1930's. This alloy is widely used in structural aerospace applications and is situated in the $\alpha+S$ phase field as shown in Fig. 1. For car body, possible new alloys around Al–(0·2–0·6)Cu–(1–4)Mg (wt-%) are in development as a substitute for Al–Mg–Si. In answer to the requirement for new light weight strength alloys in the aerospace industry, the Al–Cu–Mg alloys with addition of lithium such as 209x and 809x alloys have been developed, and have seen some limited but growing usage in the past decade.

Based on the functions they perform and the temperature ranges in which they form, the secondary phases in Al based alloys are generally subdivided into three classes: constituent particles, dispersoids and precipitates. Constituent particles are phases that form by a liquid–solid eutectic reaction during solidification and which may transform further during further higher temperature heat treatments, e.g. homogenising or solution heat treatments. In most applications, constituent phases are undesirable as they are generally detrimental to the properties, especially the damage tolerant properties. Some constituent particles (i.e. eutectic $\theta+S$ phases) can also cause localised melting at temperatures that are lower than in similar alloys which do not contain the constituent particles, which can limit high temperature thermomechanical treatments. These constituent particles are generally intermetallic phases and are often referred to as '(coarse) intermetallics'. (Note that as dispersoids and precipitates are generally also intermetallic phases, this terminology can be the source of confusion and the term of constituent phases is preferred instead.) Dispersoid particles form during the ingot homogenisation, and are generally finer than the constituent particles. In Al alloys for structural applications, their main purpose is control of the grain structure during high temperature heat treatment and thermo-mechanical treatments. The main examples are Zr, Mn, Cr and Sc containing phases. Precipitates are fine phases or clusters that form during aging.

Table 1 Nominal compositions (wt-%) of some typical Al–Cu–Mg–(Li) alloys

Alloy	Cu*	Mg*	Li*	Mn*	Zr*	Fe†	Si†	Other
2017	4·0	0·6	…	0·7	…	0·70	0·50	
2024	4·2	1·5	…	0·6	…	0·50	0·50	
2124	4·2	1·5	…	0·6	…	0·3	0·20	
2224	4·1	1·5	…	0·6	…	0·15	0·12	
2324	4·1	1·5	…	0·6	…	0·12	0·10	
2524	4·2	1·3	…	0·6	…	0·10	0·04	
2090	2·7	0·25	2·25	…	0·11	0·12	0·10	
2091	2·0	1·5	2·0	…	0·1	0·30	0·20	
2095	4·0	0·4	1·0	…	0·11	0·15	0·12	0·4Ag
2097	2·8	0·35†	1·5	0·35	0·11	0·15	0·12	0·35Zn†
8090	1·3	0·9	2·4	…	0·1	0·30	0·20	
8091	1·9	0·85	2·6	…	0·12	0·50	0·30	

*Median composition.; †maximum (except 2524: average composition given in Refs 8 and 9).

Even though Al–Cu–Mg heat treatable alloys were invented almost one century ago, and the precipitates, dispersoids and constituent particles have been studied in detail for more than half a century, many details about their existence and especially the aging sequences are still a matter of dispute. The purpose of this paper is to present a critical review of the precipitation and formation of intermetallic phases and their precursors occurring during heat treatments of dilute precipitation hardening Al–Cu–Mg based alloys, with and without Li additions.

As microstructures are highly dependent on alloy compositions, two separate sections will deal with Al–Cu–Mg with and without addition of Li. Attention will be focused on phase structure and identification.

Al–Cu–Mg alloys

Constituent phases in commercial alloys

Constituent phases (coarse intermetallic phases) form by a liquid–solid eutectic reaction during solidification and may transform on further heat treatment. In general, the particles are coarse with sizes ranging from one to several tens of micrometres. Particle size decreases as solidification rate increases, as Fe and/or Si content decrease,[4] and as the amount of deformation during mechanical and thermomechanical processing increases. Two groups of phases may be distinguished according to their stabilities in commercial alloys or related alloys: one is generally insoluble during heat treatment and the other is generally soluble provided the amount of main alloying atoms is kept below solubility limits. The insoluble phases arise mostly from Fe and/or Si impurities, which, in commercial alloys for structural applications, are very often present because of the high cost of reducing total impurity levels to below the maximum solubility levels (about 0·1 wt-%). These constituent particles are insoluble because of the low solubility of Fe in aluminium and the low solubility of Si in Al alloyed with Mg. The soluble constituent phases can be dissolved during heat treatment, by virtue of the high solubility of Cu and Mg in Al. Figure 2 shows a backscattered electron (BSE) image and the element mappings for a 2024 as cast alloy. It presents a eutectic structure containing Al, Cu, Mg, Fe and Si, and is likely

International Materials Reviews IMR413.3d 22/4/05 21:23:29
The Charlesworth Group, Wakefield +44(0)1924 369598 - Rev 7.51n/W (Jan 20 2003)

S.C. Wang and M.J. Starink, Review of precipitation in Al-Cu-Mg(-Li) alloys, Int Mater Rev., 2005, Vol. 50, pp 193-215

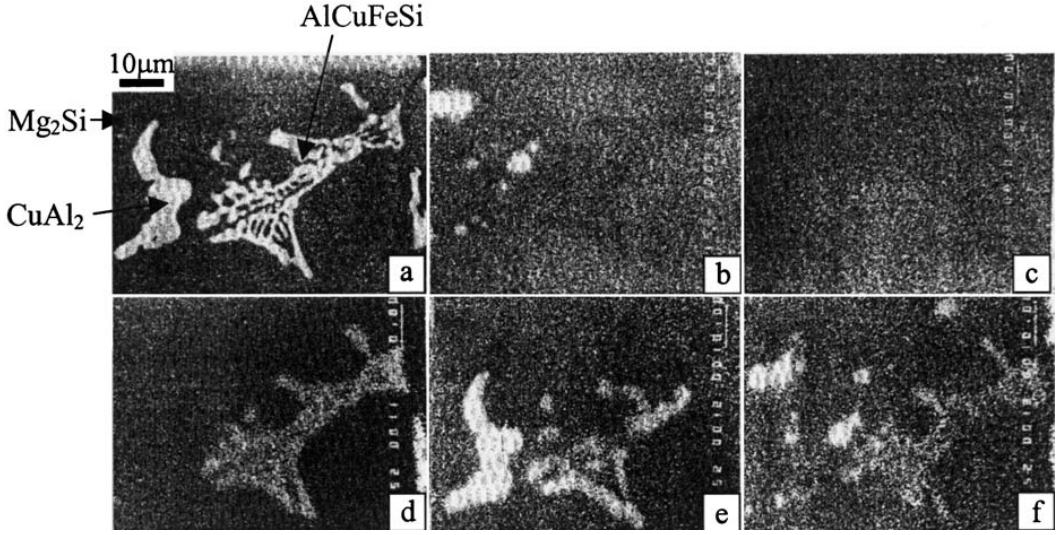

a BSE image; *b* Mg; *c* Mn; *d* Fe; *e* Cu; *f* Si

2 SEM BSE images and mapping for coarse phases in 2024 alloy (from Ref. 5)

to be a mixture of $Al_{12}Fe_3Si$, Al_7Cu_2Fe and $Al_6(Fe,Cu)$ and soluble particles Al_2Cu and Mg_2Si,[5] which is consistent with the results of Wang *et al.*[6] and Starke and Staley[2] who reported $Al_{12}(Fe,Mn)_3Si$, Al_7Cu_2Fe, $Al_6(Fe,Cu)$, Mg_2Si, Al_2Cu and Al_2CuMg in 2024 alloys. Table 2 shows their corresponding crystal structures.

The constituent phases, and especially the insoluble ones, are normally deleterious for the mechanical properties as they are the sources of crack initiation and corrosion, and enhance crack growth, while they make no substantial contribution to the yield strength of the alloy. The amount of insoluble Fe/Si particles can be reduced using alloys with enhanced purity (for example, the 2324 alloy in Table 1) and accordingly, these damage tolerance properties are improved. Figure 3 shows the effect of Fe/Si impurities on the strength and fracture toughness of 2×24 alloys (see Table 1 for compositions). This figure indicates that the fracture toughness depends largely on impurities (up to 50% increase compared to a 2024 alloy) but the strengthening is largely unaffected by impurities. Accordingly, the 2524 alloy in which Fe, Si impurities are further reduced in 2×24 alloys, has been developed by Alcoa to improve the fracture toughness and fatigue crack growth resistance of 2×24 alloys.[7–9]

Dispersoid particles

Dispersoids are formed by a solid–solid reaction during long term heat treatment (homogenisation). The main role of such dispersoids is to control grain size and resistance to recrystallisation. With sizes in the range of 0·02–0·5 μm they are much smaller than constituent particles.[2] Because of the low solubility of the main dispersoid forming elements Mn, Zr and Cr, dispersoids cannot be dissolved to an appreciable extent by subsequent solid state thermal treatments. During homogenisation, some Mn can diffuse to $Al_{12}Fe_3Si$ constituent particles to form $Al_{12}(Fe,Mn)_3Si$.[2,5,6]

In 2×24 alloys, the main dispersoid is $Al_{20}Cu_2Mn_3$ (so-called 'T phase'), which has a rodlike shape with $\langle010\rangle$ as the rod growth direction (Fig. 4*a*). The structure of $Al_{20}Cu_2Mn_3$ phase had been first proposed by Robinson[10] using X-ray diffraction (XRD) to be orthorhombic with lattice parameters a=2·42 nm, b=1·25 nm and c=0·775 nm. The possible space group for T phase was proposed to be *Bbmm*, *Bbm2* or *Bb2mb*.[10] Mondolfo[11] proposed similar lattice parameters of a=2·411 nm, b=1·251 nm and c=0·771 nm but a different space group, i.e. *Cmcm*. With the new development of convergent beam diffraction (CBD) technique in the 1980s, it was possible to unambiguously determine the structure. Wang *et al.*[12] and Li and colleagues[13,14] supported the Robinson model[10] and determined the structure as *Bbmm*. Furthermore, twins with diamond slip (i.e. ¼⟨101⟩ slip between two twins) are frequently observed in T phase as shown by the high resolution image in Fig. 4.

Table 2 Constituent phases in 2024 alloy (from Refs 6 and 11)

Phase	Structure	Lattice parameter, nm
$Al_{12}(Fe,Mn)_3Si$	$Im\bar{3}$	a=1·23
Al_7Cu_2Fe	*P4/mnc*	a=0·6336, c=1·487
Mg_2Si (β)	$Fm\bar{3}m$	a=0·6351
Al_2Cu (θ)	*I4/mcm*	a=0·6066, c=0·4874
Al_2CuMg (S)	*Cmcm*	a=0·401, b=0·923, c=0·714

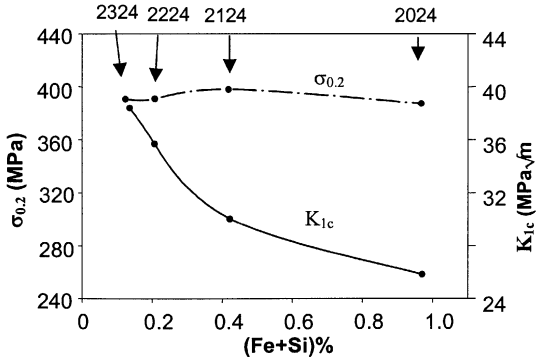

3 Effect of Fe and Si impurity contents on strength and fracture toughness of 2×24 series alloys aged at 190°C for 12 h (from Ref. 5)

International Materials Reviews IMR413.3d 22/4/05 21:23:30
The Charlesworth Group, Wakefield +44(0)1924 369598 - Rev 7.51n/W (Jan 20 2003)

S.C. Wang and M.J. Starink, Review of precipitation in Al-Cu-Mg(-Li) alloys, Int Mater Rev., 2005, Vol. 50, pp 193-215

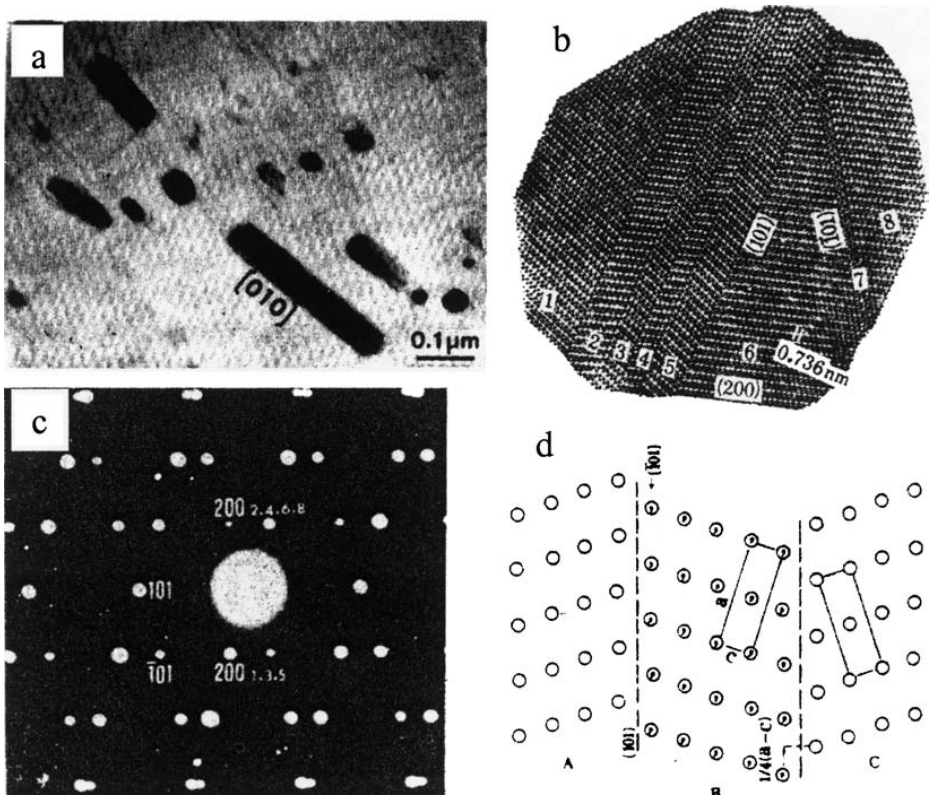

a bright field image; *b* high resolution image showing twin structure; *c* diffraction pattern corresponding to Fig. 4*b*; *d* illustration of glide reflection symmetry between neighbouring components of twins

4 $Al_{20}Cu_2Mn_3$ dispersoid phases in 2024 alloys (from Ref. 14)

Precipitates forming during aging I: S aging sequences

It should be noted that in general, no differences have been reported for the sequence of S precipitation for different alloys in the S containing phase fields of Fig. 1. For a Cu/Mg weight ratio of 2·2 (i.e. in the $\alpha+S$ phase field), Bagaryatsky[15] reported the following precipitation sequence

$$SSS \rightarrow GPB\cdot zone \rightarrow S'' \rightarrow S' \rightarrow S(CuMgAl_2)$$

where SSS stands for supersaturated solid solution. The term GPB (Guinier–Preston–Bagaryatsky) zones first appeared in work by Silcock[16] who suggested they might be different to the GP (Guinier–Preston) zone in Al–Cu alloys, which had been discovered earlier. Whilst the above sequence has been often cited, the structure of the phases has proved controversial. In the following, the identification of these phases and their interrelations are critically reviewed.

S'/S phase

On the basis of XRD work, Perlitz and Westgren[17] (PW) first proposed S (Al_2CuMg) as having a *Cmcm* structure with lattice parameters a=0·400 nm, b=0·923 nm, c=0·714 nm, as shown in Fig. 5*a*. Table 3 shows its space group and atomic positions.[18] Since then, two other models have been reported for the S phase:[11,19] Mondolfo[11] suggested a modified PW model in which some Cu and Mg atomic coordinates were changed as shown in Fig. 5*b* (please note that the modified structure does not belong to *Cmcm* as claimed[11]). Jin *et al.*[19]

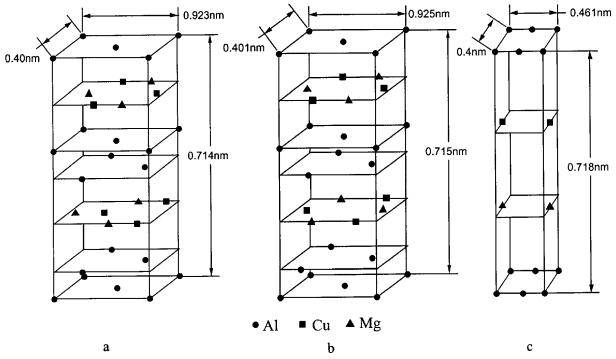

a Perlitz and Westgren model (from Ref. 17); *b* Mondolfo model (from Ref. 11); *c* Jin, Li and Yan model (from Ref. 19)

5 Proposed models for S phase

Table 3 Space group and atomic positions of S phase (from Ref. 18)

Phase	Structure	Lattice parameter, nm	Multiplicity/Wyckoff letter	Positions			Occupancy
				x	*y*	*z*	
S	*Cmcm*	*a*=0·400	4c	0	0·778	0·25	100%Cu
		b=0·923	4c	0	0·072	0·25	100%Mg
		c=0·714	8f	0	0·356	0·056	100%Al

International Materials Reviews IMR413.3d 22/4/05 21:23:39
The Charlesworth Group, Wakefield +44(0)1924 369598 - Rev 7.51n/W (Jan 20 2003)

S.C. Wang and M.J. Starink, Review of precipitation in Al-Cu-Mg(-Li) alloys, Int Mater Rev., 2005, Vol. 50, pp 193-215

proposed an orthorhombic structure with space group *Pmm2*, lattice parameters a=0·4 nm, b=0·461 nm and c=0·718 nm as shown in Fig. 5*c*. Al-Khafaji *et al.*[20] found that only the PW model[17] gave results consistent with their HREM (high resolution electron microscope) images. Radmilovic and Kilaas[21,22] found the PW model matched their HREM images better than the other previously proposed models in Fig. 5, but suggested a modified model that provides an even better match. The model of Radmilovic and Kilaas is identical to the PW model except that Cu and Mg atoms are interchanged. However, this modified PW structure was rejected by Wolverton,[23] because his first principles calculation indicated that that it would cause much higher energy than the PW model and was therefore unstable.

To explore this further, measured diffraction patterns and diffraction simulations will be compared. First it should be noted that in precipitation heat treatments, the S phase forms as laths on $\{210\}_{Al}$ habit planes and is elongated along $\langle 100\rangle_{Al}$. The orientation relationship between S and the Al matrix is[15]

$$[100]_{Al}//[100]_S,[02\bar{1}]_{Al}//[010]_S,[012]_{Al}//[001]_S \quad (1)$$

Thus, 12 equivalent variants to the above orientation relationship exist. The corresponding directions of these variants parallel to $[100]_{Al}$ can be calculated using the method suggested by Li and Yan[24] and results are shown in Table 4. The corresponding diffraction patterns for 12 variants seen from $[100]_{Al}$, as obtained from simulation using Diffract 1·2a software, are shown in Fig. 6. The strong reflections from S variants around the forbidden$\{110\}_{Al}$ can be explained well by $\{112\}_S$, $\{131\}_S$ and double diffractions. This explanation was first proposed by Gupta *et al.*[25] Figure 7*a* shows the combined diffraction patters of $[100]_{Al}$ and all 12 S variants. Figure 7*b* shows the practical diffraction patterns observed from $[100]_{Al}$,[26] which matches well to the simulated diffraction patterns as shown in Fig. 7*a*. (And simulations using the model of Radmilovic and Kilaas provide similar results.) On balance, the present review of published work indicates that the PW model is correct.

Figure 8*a* shows the morphology of S phase viewed on $\langle 100\rangle_{Al}$ with the elongated direction along $\langle 100\rangle_S$. The corresponding selected area diffraction (SAD) pattern is shown in Fig. 8*b*. As a result of the large area chosen for diffractions,[27] some weak diffractions based on simulation in Fig. 7*a* may not be observed as shown in the schematic diagram of Fig. 8*c*.

Several researchers (e.g. Bagaryastsky[15]) have reported an intermediate phase S', with only slight differences in lattice parameters differentiating the S' phase from the equilibrium phase S. S' is regarded as a precursor to the equilibrium phase S. The S' phase was reported to possess lattice parameters either $a_{S'}$=0·405 nm, $b_{S'}$=0·906 nm, $c_{S'}$=0·724 nm[11] which is coherent with the Al matrix, or $a_{S'}$=0·404 nm, $b_{S'}$=0·925 nm, $c_{S'}$=0·718 nm which is semi-coherent with the matrix (e.g. Ref. 28). The indication S' has been widely adopted to denote the needle and lath shaped semi-coherent precipitates that form during aging in Al–Cu–Mg based alloys, mostly on dislocations and solute clusters. The shapes of these precipitates are slightly different from the S phase particles, and S' and S may only be distinguished on the basis of misfit.[29] As the proposed S' structures have essentially the same crystal structures as the S phase, with very small differences in lattice parameters, this does not seem to warrant the designation of a new or separate phase. Indeed, many recent publications make no distinction between the S' and S phase. The authors believe that the stage between the so-called S' and S is continuous rather than distinct, and therefore there is no reason to use the indication S'. Instead, one may refer to precipitates previously indicated as S', as semi-coherent S.

To the authors' knowledge, there is no published time–temperature transformation (TTT) diagram for the formation of S phase. However, based on the DSC results of Starink and co-workers,[30,31] Such a curve may be presented for solution treated, water quenched and subsequently 2·5% stretched Al–2·81Cu–1·05Mg–0·41Mn (wt-%) alloy as shown in Fig. 9.

GPB2/S" phase

Bagaryatsky[15] proposed an intermediate structure, termed S", which is closely related to S and coherent with the Al rich matrix. Coherency is obtained by virtue of structure that is slightly distorted compared to the S phase,[17] and orientation relationship[32]

$$[100]_{Al}//[100]_{S''},[0,\bar{5},3]_{Al}//[011]_{S''},[0,1,1,]_{Al}//[013]_{S''} \quad (2)$$

Shchegoleva and Buinov[33] agreed that S" has similar atomic coordinates and lattice parameters to the S phase but suggested that the S" phase is in fact a monoclinic crystal with α=88·6° instead of orthorhombic to satisfy the above orientation relationships

$$[100]_{Al}//[100]_{S''},[0,7,17]_{Al}//[010]_{S''},[0,13,\bar{5}]_{Al}//[001]_{S''} \quad (3)$$

Clearly, there are some contradictions in the above two

Table 4 Twelve equivalent orientation relationships between S and aluminium matrix (based on Ref. 24)

Variant	Equivalent orientation relationship	Directions of S variants (deviation away from $[100]_{Al}$)
1	$[100]_{Al}//[100]_S$, $[02\bar{1}]_{Al}//[010]_S$, $[012]_{Al}//[001]_S$	$[100]_S$ (0°)
2	$[\bar{1}00]_{Al}//[100]_S$, $[021]_{Al}//[010]_S$, $[01\bar{2}]_{Al}//[001]_S$	$[\bar{1}00]_S$ (0°)
3	$[100]_{Al}//[100]_S$, $[0\bar{1}2]_{Al}//[010]_S$, $[02\bar{1}]_{Al}//[001]_S$	$[100]_S$ (0°)
4	$[\bar{1}00]_{Al}//[100]_S$, $[01\bar{2}]_{Al}//[010]_S$, $[0\bar{2}1]_{Al}//[001]_S$	$[\bar{1}00]_S$ (0°)
5	$[001]_{Al}//[100]_S$, $[2\bar{1}0]_{Al}//[010]_S$, $[120]_{Al}//[001]_S$	$[021]_S$ (5·4°)
6	$[00\bar{1}]_{Al}//[100]_S$, $[210]_{Al}//[010]_S$, $[1\bar{2}0]_{Al}//[001]_S$	$[021]_S$ (5·4°)
7	$[0\bar{1}0]_{Al}//[100]_S$, $[\bar{2}01]_{Al}//[010]_S$, $[\bar{1}02]_{Al}//[001]_S$	$[0\bar{2}1]_S$ (5·4°)
8	$[010]_{Al}//[100]_S$, $[\bar{2}0\bar{1}]_{Al}//[010]_S$, $[\bar{1}02]_{Al}//[001]_S$	$[0\bar{2}1]_S$ (5·4°)
9	$[00\bar{1}]_{Al}//[100]_S$, $[1\bar{2}0]_{Al}//[010]_S$, $[\bar{2}\bar{1}0]_{Al}//[001]_S$	$[01\bar{3}]_S$ (3·3°)
10	$[001]_{Al}//[100]_S$, $[\bar{1}\bar{2}0]_{Al}//[010]_S$, $[2\bar{1}0]_{Al}//[001]_S$	$[0\bar{1}3]_S$ (3·3°)
11	$[010]_{Al}//[100]_S$, $[\bar{1}02]_{Al}//[010]_S$, $[\bar{2}01]_{Al}//[001]_S$	$[0\bar{1}3]_S$ (3·3°)
12	$[0\bar{1}0]_{Al}//[100]_S$, $[102]_{Al}//[010]_S$, $[\bar{2}01]_{Al}//[001]_S$	$[01\bar{3}]_S$ (3·3°)

International Materials Reviews IMR413.3d 22/4/05 21:23:49
The Charlesworth Group, Wakefield +44(0)1924 369598 - Rev 7.51n/W (Jan 20 2003)

S.C. Wang and M.J. Starink, Review of precipitation in Al-Cu-Mg(-Li) alloys, Int Mater Rev., 2005, Vol. 50, pp 193-215

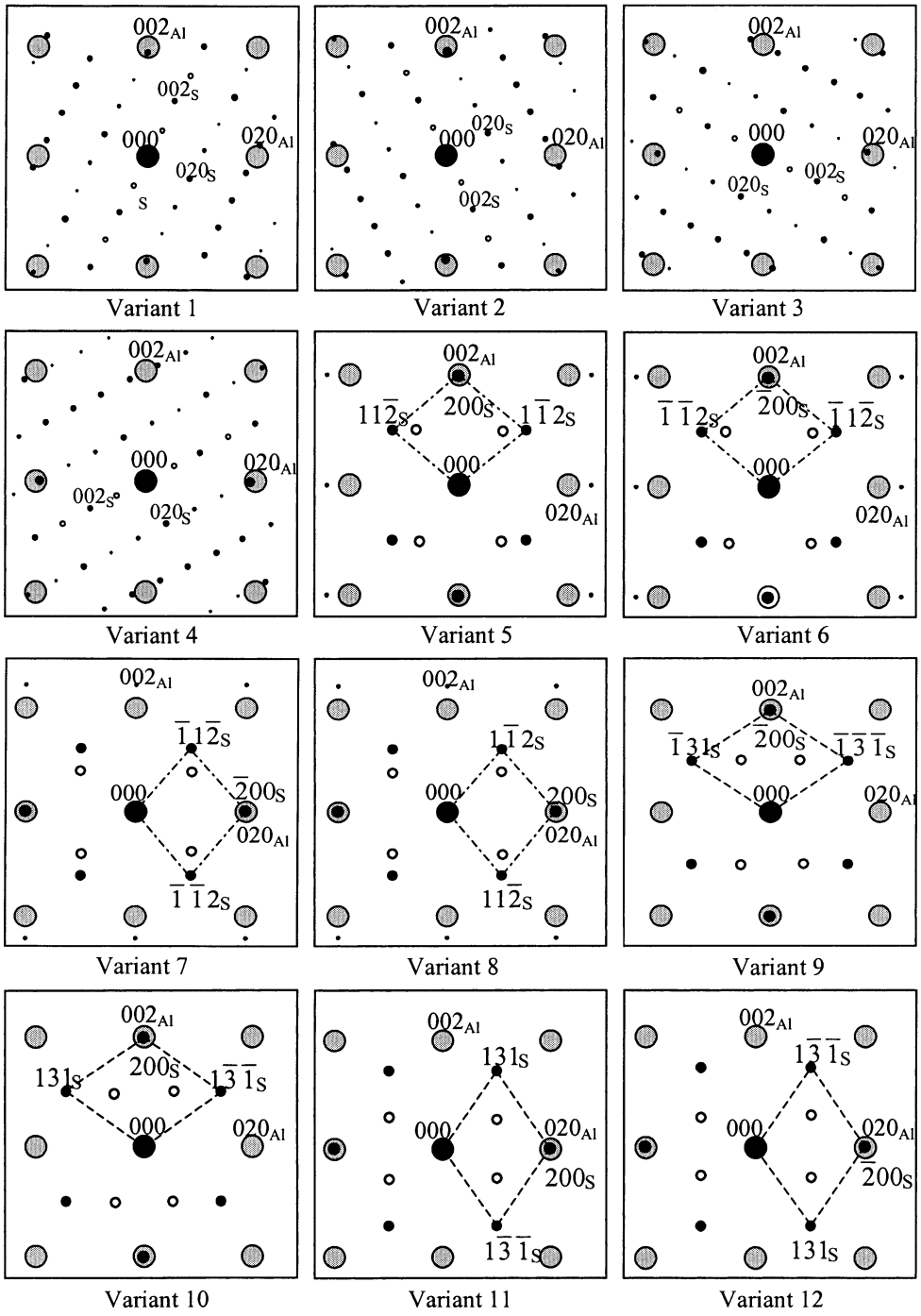

6 Simulated diffraction patterns of 12 variants of S phase observed from $[100]_{Al}$; large grey circles present Al reflections, solid circles are S phase reflections and small open circles are double diffractions (based on Ref. 24 and software Diffract 1·2a)

orientation relationships. Various other claims for the presence and structure of a distinct S" have been made. For example, in X-ray work, Silcock[16] did not observe a phase resembling the S" phase reported by Bagaryatsky.[15] Rather she suggested the existence of a structure rich in copper, more likely to be related to the compound $Al_5Cu_5Mg_2$ with cubic structure and a= 0·827 nm. Based on electron diffraction, Cuisiat *et al.*[34] suggested an S" phase as an orthorhombic structure with a=0·405 nm, b=0·405 nm and c=0·81 nm (Fig. 10*a*). Shih *et al.*[35] proposed a partially ordered so-called GPB2 zone which has a tetragonal structure and lattice parameters of a=0·58 nm, c=0·81 nm. Recently, by calculations of formation enthalpies for GPB zones and complex precipitates in Al alloys using first-principles, Wolverton[23] predicted a new structure for the GPB2 zone as a tetragonal structure with a=0·401 nm and c=0·81 nm (Fig. 10*b*). A further indication for the existence of GPB2 or S" is the Fourier transformation (FT) pattern obtained by Charai *et al.*[36] in HREM (Fig. 11) work on an Al–2·03Cu–1·28Mg (wt-%) alloy that was solution treated and aged at 200°C for 4 h. Realising that their FT patterns were not consistent with S phase, Charai *et al.* termed this phase S" phase

International Materials Reviews IMR413.3d 22/4/05 21:23:49
The Charlesworth Group, Wakefield +44(0)1924 369598 - Rev 7.51n/W (Jan 20 2003)

S.C. Wang and M.J. Starink, Review of precipitation in Al-Cu-Mg(-Li) alloys, Int Mater Rev., 2005, Vol. 50, pp 193-215

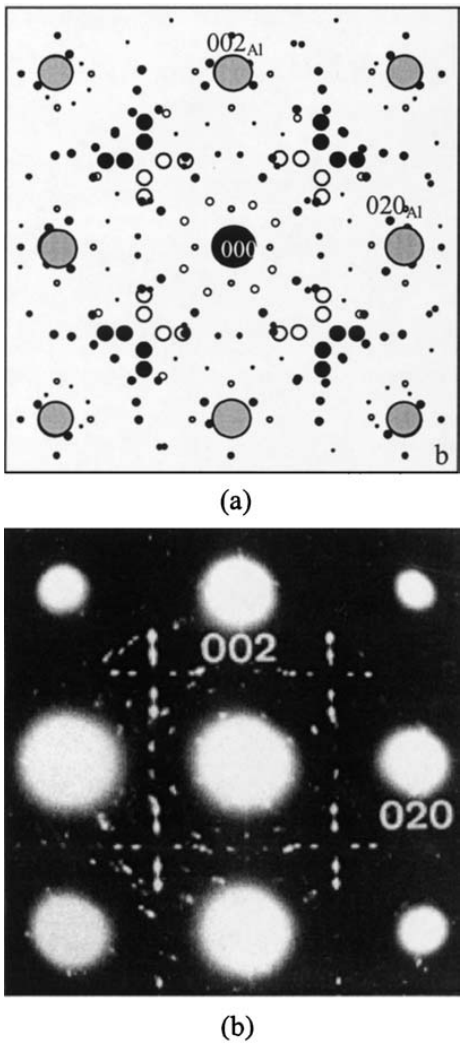

a simulated $[100]_{Al}$ diffraction patterns with reflections from all 12 variants of S phase (as shown in Fig. 6); large grey circles represent Al matrix, solid circles are S phase reflections and small open circles are double diffractions; *b* observed $[100]_{Al}$ SAD pattern for Al–4·43Cu–2·00Mg–0·53Mn (wt-%) alloy aged at 250°C for 6 h (by courtesy of Zhang *et al.* from Ref. 26)

7 Comparison of simulation and experimental electron diffraction pattern of S variants on $[001]_{Al}$

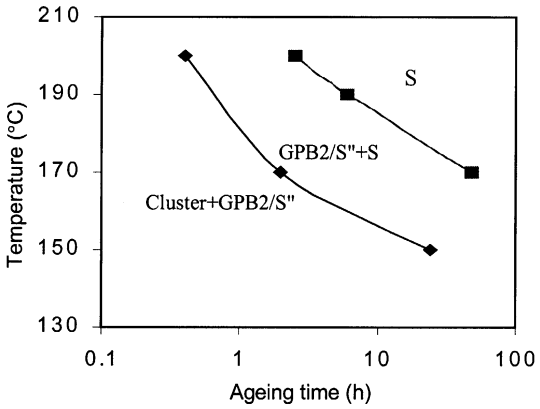

9 Time–temperature transformation diagram for formation of S phase in solution treated, water quenched and stretched Al–2·81Cu–1·05Mg–0·41Mn (wt-%) alloy based on DSC results from Refs 30 and 31; lines are drawn for 5% and 95%S phase formed

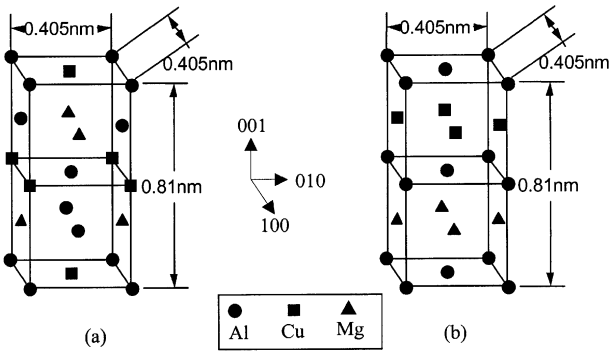

a S" structure proposed by Cuisiat *et al.* (from Ref. 34); *b* GPB2 structure proposed by Wolverton (from Ref. 23)

10 Proposed S"/GPB2 structures

suggesting a primitive monoclinic structure with a=0·32 nm, b=0·405 nm, c=0·254 nm, β=91·7°. However, none of the above structures have been independently confirmed. Despite reports of an S"/GPB2 phase,[15,16,28,34,36,37] other researchers (e.g. Wilson and Partridge[38] and Ringer and co-workers[29,39,40]) were unable to confirm the presence of the S" phase.

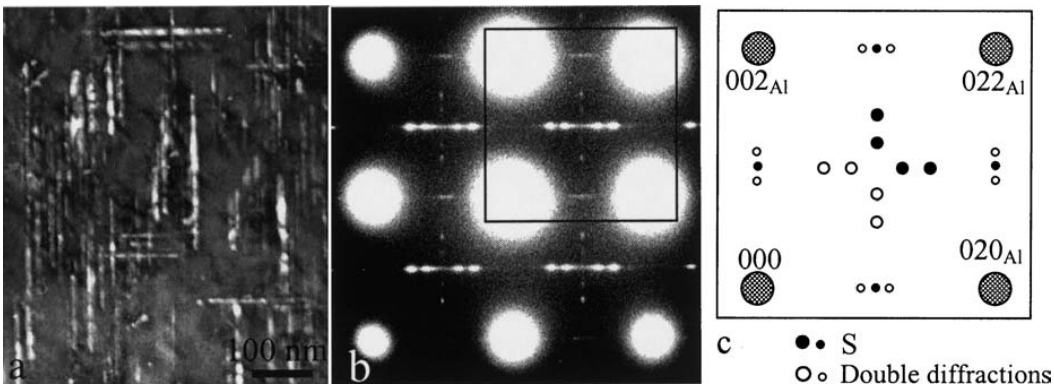

a dark field, B=$[100]_{Al}$; *b* SAD, B=$[100]_{Al}$; *c* schematic diagram of area boxed in Fig. 8b

8 TEM micrographs of Al–2·81Cu–1·05Mg–0·41Mn (wt-%) alloy solution treated, stretched and subsequently aged for 12 h at 190°C (from Ref. 30)

International Materials Reviews IMR413.3d 22/4/05 21:23:57
The Charlesworth Group, Wakefield +44(0)1924 369598 - Rev 7.51n/W (Jan 20 2003)

S.C. Wang and M.J. Starink, Review of precipitation in Al-Cu-Mg(-Li) alloys, Int Mater Rev., 2005, Vol. 50, pp 193-215

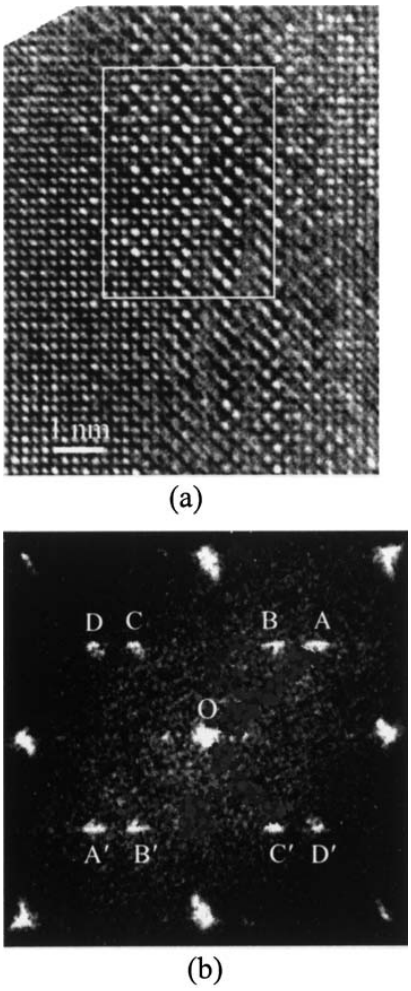

a HREM micrograph; *b* FT from frame shown in *a*

11 HREM micrograph and Fourier transformation in $[100]_{Al}$ of Al–2·03Cu–1·28Mg (wt-%) alloy aged at 200°C for 4 h (adapted from Ref. 36, by courtesy of Professor A. Charai)

The present authors[41,42] reanalysed Charai *et al.*'s data and noticed that their suggested monoclinic structure could not explain the FT pattern in Fig. 11*b* and no HREM simulation supporting such a structure was presented. A new orthorhombic structure shown in Fig. 12*a* was proposed for which pattern (Fig. 12*b*) viewed along [001] resembles the patterns seen in the HREM image in Fig. 11*a*. The corresponding diffraction pattern shown in Fig. 12*c* matches well the FT of Fig. 11*b*. The composition of the structure in Fig. 12*a* is $Al_{10}Cu_3Mg_3$, which is between that of S phase (Al_2CuMg) and Cu–Mg clusters which have about 90%Al.[30] The orientation relationship between GPB2/S" and Al matrix satisfies

$$[100]_{GPB2/S''}//[100]_{Al}, [010]_{GPB2/S''}//[010]_{Al},$$
$$[001]_{GPB2/S''}//[001]_{Al} \quad (4)$$

Through calculation of its structural factors, the diffraction patterns for all six independent variants of GPB2/S" precipitates in $[001]_{Al}$ were predicted. These variants explain well the diffraction pattern observed in the Al–Cu–Mg aging stage before the formation of S phase.[42]

There have been experimental indications from DSC work[43] to show that stretch before aging could hinder or reduce the formation of GPB2/S". As shown in Fig. 13, there is an exothermic effect which was attributed[43] to the formation of GPB2/S" in an Al–Cu–Mg alloy without deformation, and such peak is not present if the alloy is stretched by 2% before artificial aging. It should be noted however that these DSC experiments are merely indications, and they cannot prove or disprove GPB2/S" formation.

The relation between GPB2/S" and S phase is not clear. However, the work of Charai *et al.*[36] on quenched and aged alloys and recent TEM and DSC work[44] on quenched and subsequently stretched (2·5%) and aged alloys show these phases co-exist and the S phase may consume GPB2/S" on further aging. For example, after aging the stretched Al–2·81Cu–1·05Mg–0·41Mn (wt-%) alloy for 24 h at 150°C, TEM with SAD reveals faint reflections which are considered to be because of very fine GPB2/S"+S phase (the images cannot be resolved in conventional TEM) (Fig. 14*a–c*). After aging for 48 h as shown in Fig. 14*d–f*, a dense precipitation of S phase has occurred, and the intensity of diffractions from GPB2/S" seems to be reaching a maximum. After aging for 72 h which is close to the second stage of hardening, GPB2/S" reflections are weak and more S precipitates form and the S spots in SAD patterns have now become sharper (Fig. 14*g* and *i*). At the stage of completion of S formation (190°C for 12 h as shown in Fig. 8), only S phase spots were confirmed. Figure 15 shows the corresponding DSC thermograms of this stretched Al–2·81Cu–1·05Mg–0·41Mn (wt-%) alloy after aging for several time intervals at 150°C. Two thermal effects are normally observed in the range 150–400°C. One is a dissolution effect in the range of 200–250°C, which has been mostly referred to as being due to the dissolution of GPB zones. However, up to 48 h aging at 150°C, the heat content of this endothermic effect increases with aging time. From the above TEM results (Fig. 14), it appears that dissolution of Cu–Mg clusters causes the endothermic effect in solution treated samples, and the increasing heat content may be attributed to the dissolution of GPB2/S" which forms during aging at 150°C for up to 48 h. This conclusion is consistent with DSC results on other stretched Al–Cu–Mg alloys[30] (the additional endothermic heat flow may depend on the composition and aging temperature). The exothermic effect at 250–300°C is as a result of the formation of S phase, which shows the amount of S phase increases with aging at 150°C. The DSC curves in Fig. 15 show that when the S phase formation is completed (12 h at 190°C), the dissolution effect of clusters and GPB2/S" has completely disappeared, evidencing the complete transformation of these metastable structures into S.

In a study of an Al–0·6Cu–4·2Mg (wt-%) alloy (composition in the $\alpha+S+T$ phase field), Ratchev *et al.*[28,45] found weak spots as shown in Fig. 16*a*. For added clarity, Fig. 16*b* shows a schematic diagram of this diffraction pattern. Ratchev *et al.*[28,45] attributed these reflections (solid circles in Fig. 16*b*) to an S" phase with structure as proposed by Cuisiat *et al.*[34] However, the theoretical calculation[41,42] of the diffraction pattern using structural factors for the model of Cuisiat *et al.*[34] does not match such pattern. Interestingly, similar patterns have also been observed in other alloys with compositions well outside the S phase field. For example, such reflections have been observed in an Al–3·0 wt-%Cu

International Materials Reviews IMR413.3d 22/4/05 21:24:08
The Charlesworth Group, Wakefield +44(0)1924 369598 - Rev 7.51n/W (Jan 20 2003)

S.C. Wang and M.J. Starink, Review of precipitation in Al-Cu-Mg(-Li) alloys, Int Mater Rev., 2005, Vol. 50, pp 193-215

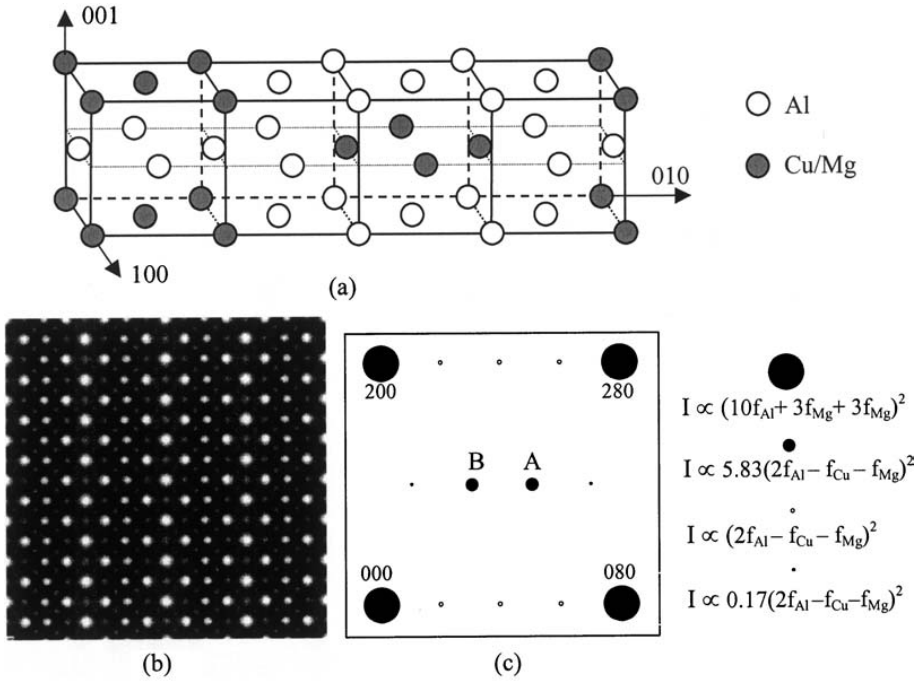

a proposed model for GPB2/S"; *b* HREM simulation along [001] with defocus at 68 nm and thickness of 4 nm; *c* simulated diffraction pattern; sizes of spots are proportional to diffraction intensities (*I*) in which f_{Al}, f_{Cu} and f_{Mg} are atomic scattering amplitudes

12 Proposed structure of GPB2/S" and corresponding simulation of HREM and diffraction pattern on [001] (from Refs. 41 and 42)

alloy[46] (the aging sequence leads to θ-Al_2Cu) and an Al–Zn–Mg–Cu alloy[47] (the aging sequence leads to η-$MgZn_2$), which are interpreted to be an oxide layer with structure of $\alpha-Al_2O_3$[46] and γ-Al_2O_3,[47] respectively. Park and Ardell[47] attributed the formation of these oxides to the electropolishing during TEM sample preparation, as no such reflections were found in the ion-beam milled samples. But, in recent HREM work on Al–0·4Cu–3Mg–0·12Si (wt-%), Kovarik *et al.*[48] obtained an FT consistent with Fig. 16, which indicates that such weak reflections did arise from precipitates. Kovarik *et al.*[49] ascribed their observations to a fully coherent, orthorhombic phase that precipitates in a quenched and aged 'Cu lean' Al–3Mg–0·4Cu–0·12Si (wt-%) alloy, which is different to the GPB2/S" phase in the 'Cu rich' Al–Cu–Mg alloys described above. These precipitates in the Cu lean alloys were termed GPBII, and they were readily observed in conventional TEM and HREM. The diffraction information from this phase can be explained in terms of orthorhombic crystal structure *Cmmm*, with lattice parameters a=1·212 nm, b=0·404 nm and c=0·404 nm.[49]

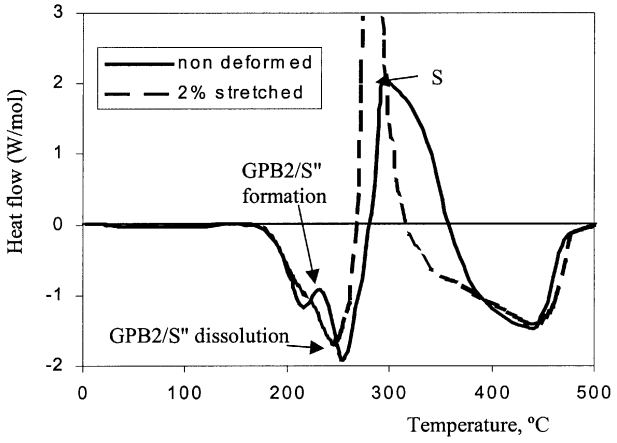

13 DSC scans, at 20 K min^{-1}, of non-deformed and 2% stretched Al–2·1Cu–1·3Mg–0·09Zr (wt-%) samples; solid line represents a sample that was solution treated (at 500°C), water quenched and then aged at 100°C for 8 days; dashed line represents a sample that was solution treated (at 500°C), water quenched, 2% stretched and then aged at 100°C for 8 days (adapted from Ref. 43)

GPB zones/Cu–Mg clusters

Evidence for the existence of the GPB zones was initially based on interpretations of weak diffraction effects arising from diffuse X-ray scattering.[15,16] In various publications, the activation energies for this reaction have been determined within the range 51–64 kJ mol^{-1}.[50–52] Bagaryatsky[15] considered the zone characteristics to be associated with short range ordering along the $\{100\}_{Al}$ planes. Gerold and Haberkorn[53] proposed a tetragonal CuAuI type structure, in which layers of Al and Cu+Mg alternately arrange along $\langle 100 \rangle$ matrix directions. Later, again based on X-ray techniques, Silcock[16] proposed zones to be small cylinders, 1–2 nm in diameter and with lengths ranging from 4 nm to more than 8 nm, depending on quenching rate. She proposed the structure to be tetragonal with a=0·55 nm, c=0·404 nm. In fact, this structure is quite unlikely as it is not coherent with the matrix and therefore a high strain will be expected. Based on the orientation relationship between matrix and semi-coherent S, Mondolfo[11] proposed that GPB zones consisted of one layer of Cu, one layer of Mg and two

International Materials Reviews IMR413.3d 22/4/05 21:24:13
The Charlesworth Group, Wakefield +44(0)1924 369598 - Rev 7.51n/W (Jan 20 2003)

S.C. Wang and M.J. Starink, Review of precipitation in Al-Cu-Mg(-Li) alloys, Int Mater Rev., 2005, Vol. 50, pp 193-215

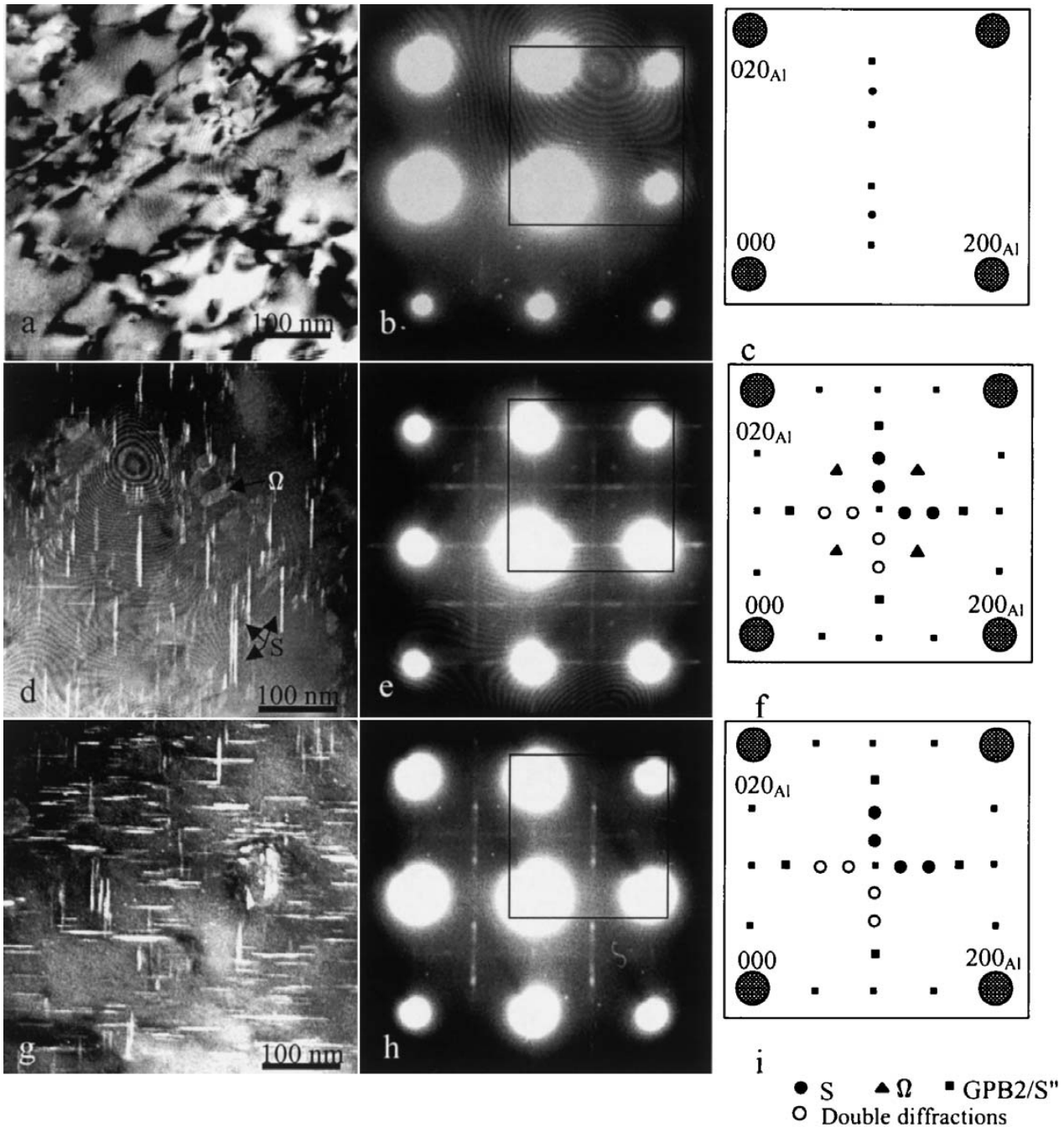

a–c 24 h; *d–f* 48 h; *g–i* 72 h

14 TEM dark field image and corresponding diffraction patterns of Al–2·81Cu–1·05Mg–0·41Mn (wt-%) alloy aged for different times at 150°C (from Ref. 44)

layers of Al, alternating along the ⟨021⟩ matrix direction. Recent first principles energy calculations by Wolverton,[23] suggested that the GPB zones could correspond to a Cu or Mg monolayer along ⟨100⟩ as a result of GPB/matrix interfacial energy.

However, none of the models for GPB zones mentioned above have been confirmed by diffraction in selected area diffraction in TEM or by phase contrast in HREM. This is in contrast to Al–Cu alloys, where the GP zones give strong strain contrast in conventional TEM and HREM[29] [caused by the smaller radius of Cu atoms (0·128 nm) than Al atoms (0·143 nm)] and show characteristic streaking in SAD along $\langle 100 \rangle_{Al}$ (caused by the GP zone formed on the $\{100\}_{Al}$ plane). The limited contrast of GPB zones could be because of the size effects of Cu and Mg atoms (radius 0·160 nm) counteracting each other, however the most probable explanation for the absence of characteristic streaking in SAD is that Cu and Mg solute atoms cluster in a random manner rather than in certain specific planes. Since the formation of co-clusters was proposed as an explanation for rapid hardening,[39] there has been considerable renewed interest in this hardening stage. For alloys with compositions within the $\alpha+S$ phase field, low temperature aging (depending on alloy, below about 160–200°C) results in a rapid hardening reaction. This rapid hardening stage accounts for approximately 60% of the total hardness increase during aging (for example, this rapid hardening is completed within 1 min for aging at 150°C shown in Fig. 17[54,55]). During this

International Materials Reviews IMR413.3d 22/4/05 21:24:20
The Charlesworth Group, Wakefield +44(0)1924 369598 - Rev 7.51n/W (Jan 20 2003)

S.C. Wang and M.J. Starink, Review of precipitation in Al-Cu-Mg(-Li) alloys, Int Mater Rev., 2005, Vol. 50, pp 193-215

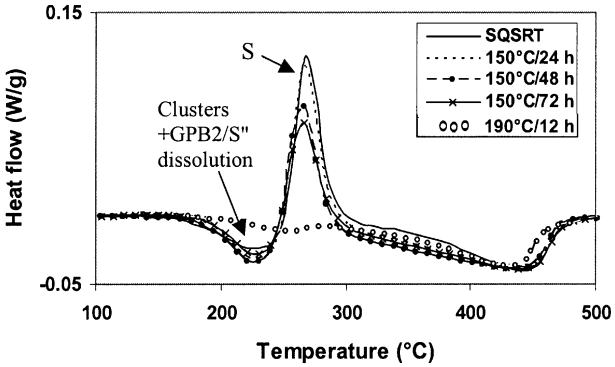

15 DSC thermograms for solution treated, quenched, stretched and subsequently aged Al–2·81Cu–1·05Mg–0·41Mn (wt-%) alloy, aged for various times (from Ref. 30); SQSRT=solution treated, quenched, stretched and subsequently room temperature aged (several months)

rapid hardening, no distinct precipitate can be detected by conventional TEM but DSC experiments clearly show a dissolution effect evidencing that a metastable pre-precipitate has formed[56] as shown in Fig. 18 (peak I). The HREM images failed to provide more information than conventional TEM, which indicates that the pre-precipitate in this stage was a random arrangement.

The difference between Cu–Mg clusters (or vacancy–Mg–Cu complexes) and GPB zones is not very clear. It has been suggested that this distinction can be made on the basis of size, shape, composition, degree of order, orientation and structure.[29] However, no distinct differences in shape, composition, degree of order, orientation and structure between these types of early pre-precipitates have been reported, and hence this criterion does not provide any clear information allowing the distinction of clusters and GPB zones. Although the vacancy–Mg–Cu complexes have been considered as precursors of GPB zones,[29] atom probe field ion microscopy (APFIM) and three-dimensional atom probe (3DAP) show no difference between zones and clusters except different sizes corresponding to the different aging temperatures or times.[30] Hence, on balance, the evidence for the existence of Cu and Mg containing GPB zones that have internal order and/or a distinct shape (such as suggested in early works by

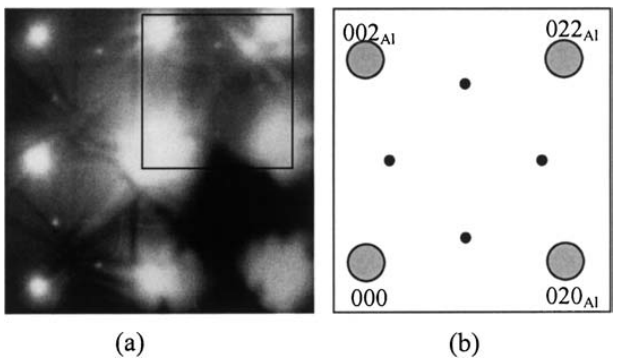

a $[100]_{Al}$ diffraction; *b* schematic diagram

16 SAD pattern for Al–0·6Cu–4·2Mg alloy (wt-%) aged at 180°C for 34 h (by courtesy of Dr P. Ratchev from Ref. 28)

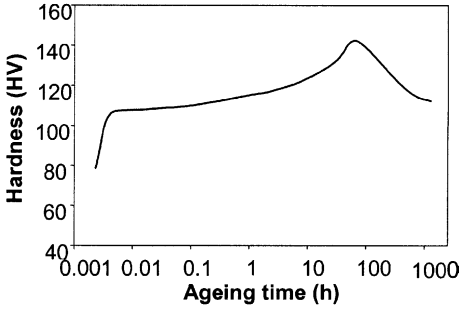

17 Age hardening curve for solution treated and quenched Al–2·55Cu–1·49Mg (wt-%) alloy aged at 150°C (from Ref. 54)

Silcock[16] and Gerold[53]) that distinguishes them from Cu–Mg co-clusters is weak.

The present assessment indicates that the range notations used for the precipitates in Al–Cu–Mg alloys have become quite confusing with at least six names being used, whereas only three different stages can be distinguished: co-clusters/GPB, GPB2/S" and S'/S. The precipitation sequence could be described as

$$SSS \rightarrow \text{co-clusters/GPB} \rightarrow /\text{GPB2}/S'' \rightarrow S'/S$$

In interpreting this sequence, it should be further noted that GPB2/S" is fully coherent with the Al-rich phase and can thus potentially form either by ordering followed by long-range diffusion (spinodal decomposition) or by long-range diffusion (clustering) followed by ordering. In the latter mechanism, the early stage of GPB2/S" phase would be expected to involve the formation and growth of clusters without distinct order, and the co-cluster stage can be explained as a stage in the formation of the GPB2/S" phase. In a pure spinodal decomposition mechanism, ordering would occur before composition variations occur, and hence a co-clustering stage would not occur as part of GPB2/S" formation.

Precipitation strengthening

Coarse constituent phases have little direct effect on the strength of Al–Cu–Mg alloys, and the strength depends largely on precipitates formed during aging. The identity of the strengthening precipitate phases in individual alloys is determined to a large extent by the Cu/Mg ratio

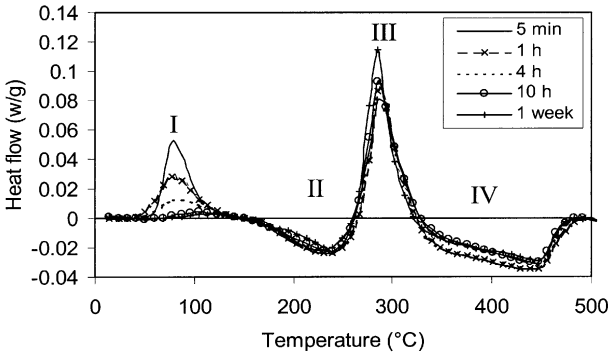

18 DSC thermograms of solution treated and quenched Al–2·81Cu–1·05Mg–0·41Mn (wt-%) alloy after aging for several intervals at 25°C; I, formation of clusters; II, dissolution of clusters and GPB2/S"; III, formation of S precipitates; IV, dissolution of S precipitates (from Ref. 31)

International Materials Reviews IMR413.3d 22/4/05 21:24:25
The Charlesworth Group, Wakefield +44(0)1924 369598 - Rev 7.51n/W (Jan 20 2003)

S.C. Wang and M.J. Starink, Review of precipitation in Al-Cu-Mg(-Li) alloys, Int Mater Rev., 2005, Vol. 50, pp 193-215

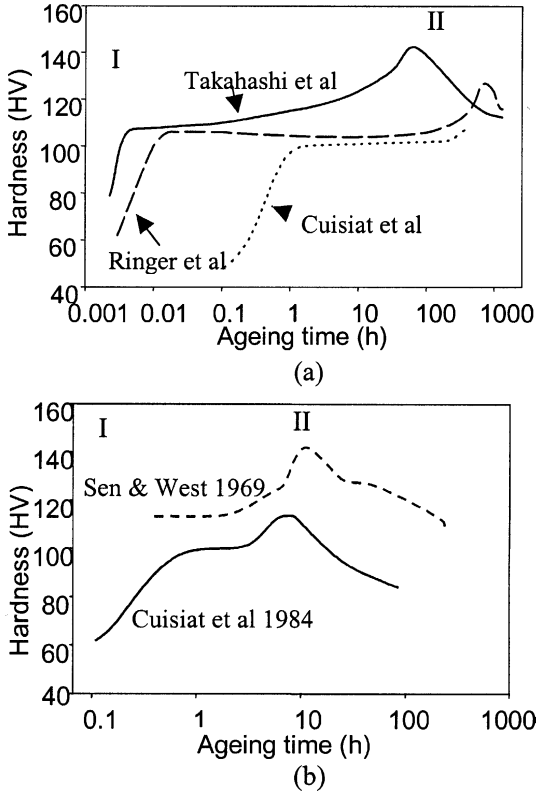

a aging at 150°C for Al–2·55Cu–1·49Mg (wt-%) (from Ref. 29), Al–2·55Cu–1·49Mg (wt-%) (from Ref. 54), and Al–2·8Cu–1·4Mg (wt-%) (from Ref. 34); *b* aging at 190°C for Al–3·3Cu–1·6Mg (wt-%) alloy (from Ref. 57) and Al–2·8Cu–1·4Mg (wt-%) (from Ref. 34)

19 Hardness versus aging time curves for several Al–Cu–Mg alloys

as shown in Fig. 1. Figure 19*a*, *b* shows the hardness versus aging time at 150°C and 190°C for selected Al–Cu–Mg alloys in the $\alpha+S$ phase field.[29,34,54,57] For all alloys, two stages of hardening occur: initial rapid hardening in a first stage (I), a plateau phase followed by a hardening peak in the second stage hardening (II).

Up to the mid 1990's, the first stage of hardening in Al–Cu–Mg alloys was generally attributed to the formation of GPB zones, whereas the second stage of hardening was generally attributed to the formation of the S phase (often indicated as S').[16,58] Since the mid 1990's, several researchers have ascribed the first stage of hardening to Cu–Mg clusters[29,40] or vacancy–Mg–Cu complexes.[55,59] (But as described above, the distinction between clusters and GPB zones is not clear.) Ringer and co-workers[29,40] used APFIM to reveal Cu–Mg clusters typically 1 nm (10–40 atoms), which were not resolved in TEM. In these studies, the co-clusters were held responsible for the rapid hardening reaction.[29,40] These co-clusters were also observed by 3DAP in two Al–Cu–Mg alloys aged at 150°C for 12 h.[30] But Reich *et al.*[60] interpreted their 3DAP work to indicate that neither clusters, GPB or precipitates are the origin of the initial rapid hardness increase, and suggested that the initial hardening is most likely to originate from solute–dislocations interactions as a result of enrichment of Mg–Mg and Cu–Cu atoms. (It was suggested[61] that this difference in interpretation could be related to the difficulty of proving a solute clustering reaction involving only a few atoms from the concentration profile of alloy containing a few atomic per cent solute level, because even statistical fluctuations may look like clusters.) Based on HREM and DSC studies, Charai *et al.*[36] further suggested that Mg–Mg aggregates were the first to appear followed by Cu–Cu aggregates and Cu–Mg clusters because of the higher binding energy between Mg atoms and vacancies and the lower activation energy for Mg diffusion in Al. Using positron spectroscopy,[55,59] vacancy–Mg–Cu complexes are the origin of the initial rapid hardening. In this mechanism, Cu and Mg solute atoms segregate to the dislocations (especially dislocation loops), locking dislocations and increasing the hardness. Recently, the proposed mechanisms of rapid hardening were critically reviewed and it was concluded that a hardening mechanism based on the difference in modulus between co-clusters and the Al rich phase was the likely cause for hardening.[31]

Several interpretations have been proposed for the causes of the second hardening stage. HREM experiments on quenched and subsequently artificially aged (not stretched) alloys have been interpreted to show that the second stage of hardening is because of GPB zones.[29,62] However, the most compelling evidence is obtained from studies combining DSC, TEM and hardness data,[30,35,63] which indicate that S phase dominates the precipitation hardening in the peak aged condition both for stretched and non-stretched alloys. The DSC studies[30,35,63] consistently show that on aging stretched and non-stretched alloys to peak hardness, the S phase precipitation peak observed in DSC virtually disappears and that the free energy of the sample substantially decreases compared to the as quenched state and the quenched and room temperature aged state to become almost equal to that of the overaged state. This shows that in the peak aged condition, a precipitate structure has nearly reached thermodynamic equilibrium. Both for stretched and non-stretched alloys, TEM evidences the existence of S phase at the peak aged condition.[30,35,63] This shows that S phase formation dominates the second stage of hardening. However, even though the amount of S phase present is close to equilibrium, some GPB2 or GPB zones may still be present, as suggested by four independent observations on various peak aged alloys: the presence of a small residual GPB2 dissolution effect in DSC curves,[35] a mottled background structure observed by TEM,[35] HREM observations of small precipitates showing no clear crystal planes which were attributed previously to GPB zones[29] and model predictions showing that some precursor structures remain present.[63] It should be noted that the evidence for the presence of substantial amounts of zones, sufficient to be the main cause of the hardening in (close to) peak aged samples,[29,62] is not conclusive. For example, the insert SAD pattern in Fig. 7*a* of the paper by Ringer *et al.*[29] shows reflections mainly from S but they link strengthening to the faint additional diffraction effects which were ascribed to GPB zones. In rationalising the various DSC, TEM and HREM observations from the different researchers,[29,30,35,63] it is further suggested that HREM images of precipitates showing no clear crystal planes which were attributed previously to GPB zones[29] might be small S precipitates (possibly with internal defects) observed in directions where a deviation between the lattices of Al and S phase exists (5·4° or 3·3°, see Table 4).

International Materials Reviews IMR413.3d 22/4/05 21:24:28
The Charlesworth Group, Wakefield +44(0)1924 369598 - Rev 7.51n/W (Jan 20 2003)

S.C. Wang and M.J. Starink, Review of precipitation in Al-Cu-Mg(-Li) alloys, Int Mater Rev., 2005, Vol. 50, pp 193-215

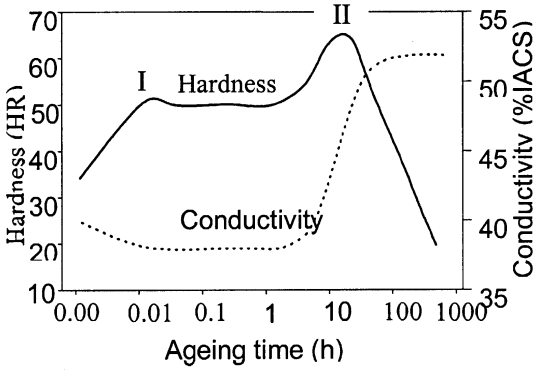

20 Electrical conductivity and Rockwell hardness versus aging time at 190°C for Al–2·62Cu–1·35Mg (wt-%) alloy (adapted from Ref. 35)

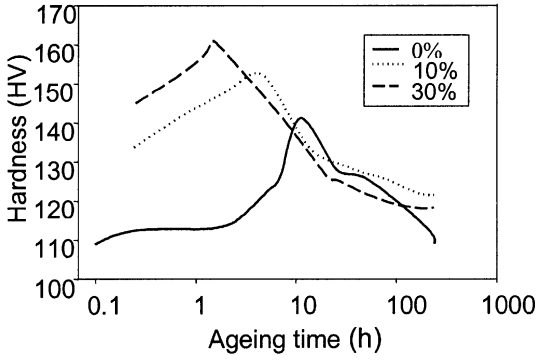

21 Hardness versus aging time curves for Al–3·3Cu–1·6Mg (wt-%) alloy aged at 190°C following deformation of solution-treated materials (from Ref. 57)

Our present analysis of published work suggests that aging in stretched alloys is predominantly related to cluster (or zone) and S phase formation which is also consistent with conductivity changes in an Al–2·62Cu–1·35Mg (wt-%) alloy on aging at 190°C after solution treatment (no stretch) shown in Fig. 20 (based on data from Ref. 35). At the first stage of hardening, the conductivity decreases as Cu–Mg clusters form (Cu and Mg have different atomic size with Al causing lattice strains). During the plateau stage, the conductivity is about constant which indicates that little change occurs, which can be as a result of growth of Cu–Mg clusters and GPB2/S" being very slow (and the composition of Cu–Mg clusters may be similar to GPB2/S"). The end of the plateau stage and the increase to peak hardness is related to a strong increase in conductivity. This strong increase in conductivity can only be due to a strong reduction of the amount of solute dissolved in the Al rich phase, which is consistent with S phase formation. Further aging causes precipitate coarsening, which increases the distance between the precipitates, making dislocation bowing easier and causes the hardness to decrease.

Deformation slows down the formation of Cu–Mg clusters, because of annihilation of quenched-in vacancies, while it introduces more heterogeneous nucleation sites for S phase. Accordingly, the strength increases with deformation as the S phase is the major strengthening precipitate and the peak for the S formation shifts to lower temperature with increasing deformation[57] as shown in Fig. 21. The formation of Cu–Mg clusters has been reported to be strongly dependent on the amount of quenched-in vacancies, as is indicated by the occurrence during DSC of a strong exothermic effect after rapid cooling (water quenching) whereas the peak was almost absent after slow cooling (compressed air cooling, 30 K s^{-1}).[45]

T phase in α+S+T phase field

The T phase has a composition of Al_6CuMg_4 and cubic structure with a=1·425 nm. The alloys within the α+S+T phase field have slow rates of softening at elevated temperatures, however, their commercialisation has been limited because their tensile strengths are not greater than alloys in the α+S phase field. Hence, very little characterisation work has been completed on alloys in this phase field.[62]

σ precipitate in Al–Cu–Mg–Si(Ag) alloys

The σ-phase has a complex cubic structure ($Pm\bar{3}$) with 39 atoms per unit cell and a lattice parameter of 0·831 nm.[64] It has been reported to be semi-coherent with a misfit of 2·8%, and to posses a cubic–cubic orientation relationship with the Al matrix.[64] The σ-phase has been observed in several overaged Al–Cu–Mg alloys, and is thought to require a minimum concentration of Si in solid solution,[65,66] although others have reported that Ag may have a similar effect.[67,68] The precipitated σ-phase exhibited better resistance to coarsening than S phase and could provide the basis of superior precipitation hardening alloys.[69]

Precipitates forming during aging II: θ precipitate sequence

The θ precipitation sequence may appear in Al–Cu–Mg alloys with compositions in the α+θ+S and α+θ phase fields. In most publications since the 1950s, the precipitation sequence is given as:[70] GPI→GPII(θ")→θ'→θ.

The metastable solvi of these precipitates in binary Al–Cu alloys are shown in Fig. 22.

θ phase

The θ phase is incoherent with the Al rich matrix and has a *I4/mcm* structure with a=0·6067 nm and c=0·4877 nm. Table 5 shows its atomic coordinates.[71]

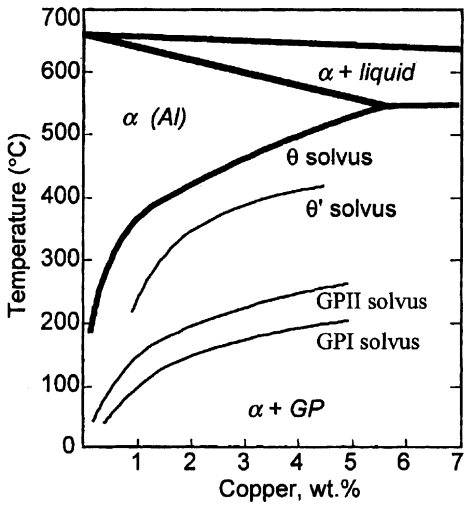

22 Al–Cu phase diagram showing metastable solvus boundaries for GP zones, θ" and θ (from Ref. 62)

International Materials Reviews IMR413.3d 22/4/05 21:24:29
The Charlesworth Group, Wakefield +44(0)1924 369598 - Rev 7.51n/W (Jan 20 2003)

S.C. Wang and M.J. Starink, Review of precipitation in Al-Cu-Mg(-Li) alloys, Int Mater Rev., 2005, Vol. 50, pp 193-215

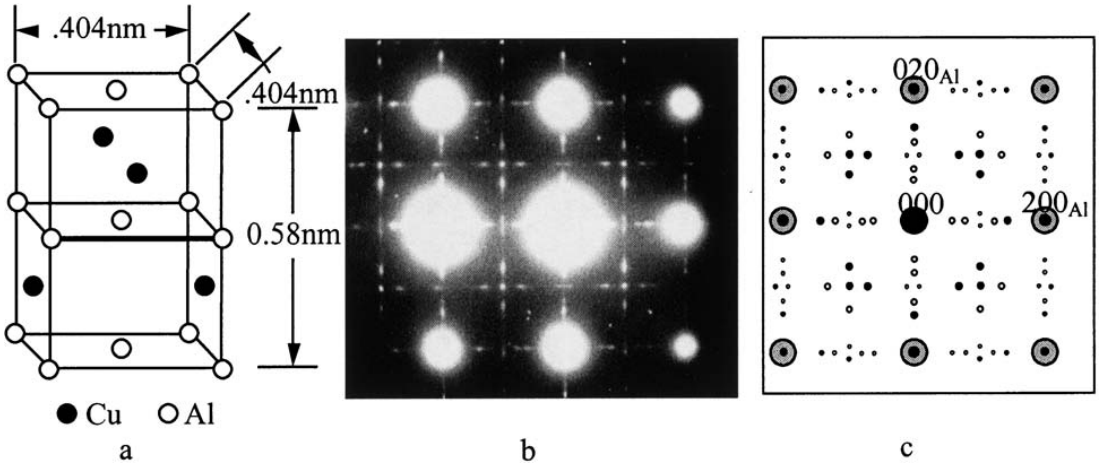

23 ***a*** **θ' structural model;** ***b*** **[001] selected area diffraction pattern aging at 160–170°C for 24 h in Al–6·2Cu–0·28Mg (wt-%) alloy (by courtesy of Papazian, from Ref. 77);** ***c*** **simulated $[001]_{Al}$ diffraction patterns with reflections from three equivalent variants of θ' phase (as shown in Fig. 24); shaded large circles represent Al reflections, solid circles are from θ' precipitate variants, and open circles are double diffractions**

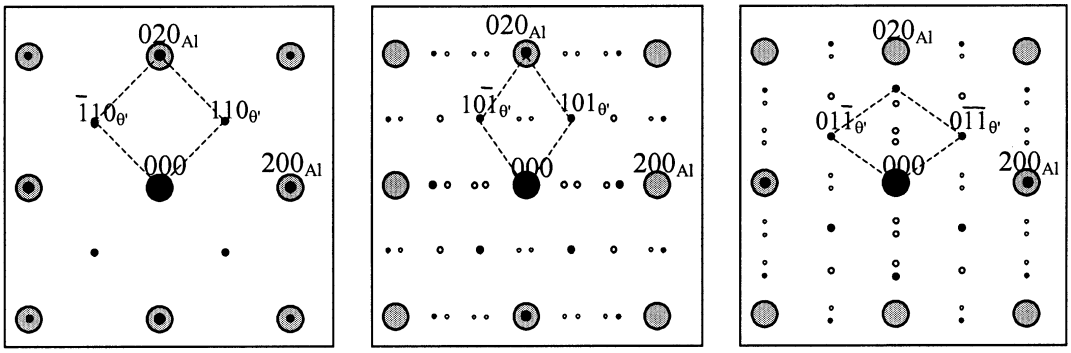

a **$[001]_{\theta'}//[001]_{Al}$;** ***b*** **$[010]_{\theta'}//[001]_{Al}$;** ***c*** **$[100]_{\theta'}//[001]_{Al}$**

24 Simulated diffraction patterns for three equivalent variants of θ' phase observed from $[001]_{Al}$; shadowed large circles represent Al reflections, solid circles are from θ' precipitate variants, and open circles are double diffractions

There are at least 22 independent orientation relationships with a matrix as summarised by Bonnet.[72]

θ' phase

The structure (Table 5) and orientation relationship of θ' originally proposed by Silcock[73] has been commonly accepted even though previously two other tetragonal structures had been proposed (a=0·82 nm, c=1·16 nm[74] and a=0·57 nm, c=0·58 nm[75]). Figure 23*a* shows the Silcock model for θ' phase with tetragonal structure and a=0·404 nm, c=0·58 nm, the space group is $I\bar{4}m2$[76] (rather than *I4/mcm* suggested elsewhere[62]) θ' phase precipitates are rectangular or octagonal plates on {100} planes and an orientation relationship with the matrix of

$$(100)_{Al}//(100)_{\theta},\ [001]_{Al}//[001]_{\theta} \quad (5)$$

Figure 23*b*[77] shows experimental SAD patterns observed from $[001]_{Al}$. Figure 23*c* shows the complex simulated diffraction patterns from three equivalent variants combined (as shown individually in Fig. 24). It is shown clearly that the simulation (Fig. 23*c*) is consistent with the SAD patterns (Fig. 23*b*).

GPI zones and GPII/θ''

The first evidence of GPI zones in room temperature aged Al–Cu alloys was provided by XRD work, which showed intensity streaks passing through the Bragg peaks in the direction of the cubic axes of the reciprocal lattice. These findings were first described independently by Guinier[78] and Preston[75] and subsequently the term Guinier–Preston zone became the established term for these phenomena. HREM[79,80] confirmed the existence

Table 5 Space group and atomic positions for θ and θ' phases

Phase	Structure	Lattice parameter, nm	Multiplicity/Wyckoff letter	Positions			Occupancy	Reference
				x	*y*	*z*		
θ'	$I\bar{4}m2$	a=0·404 c=0·58	2a	0	0	0	100%Al	73, 76
			2b	0	0	0·5	100%Al	
			2c	0	0·5	0·25	100%Cu	
θ	*I4/mcm* (tetragonal)	a=0·6067 c=0·4877	4a	0	0	0·25	100%Cu	71
			8h	0·1581	0·6581	0	100%Al	

International Materials Reviews IMR413.3d 22/4/05 21:24:32
The Charlesworth Group, Wakefield +44(0)1924 369598 - Rev 7.51n/W (Jan 20 2003)

S.C. Wang and M.J. Starink, Review of precipitation in Al-Cu-Mg(-Li) alloys, Int Mater Rev., 2005, Vol. 50, pp 193-215

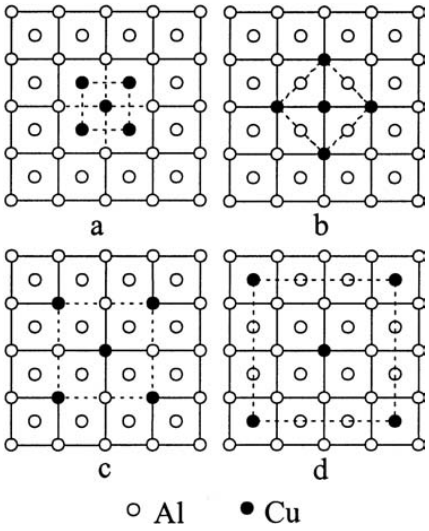

25 Atomic arrangements of GP zone formed in Al–4at.-%Cu (001) plane; Cu concentration inside GPI zone areas (dotted squares) are *a* 100 at.-%, *b* 55·5 at.-%, *c* 38·5 at.-%, and *d* 20 at.-% (from Ref. 85)

of these zones and showed that they are one Cu rich plane of atoms bounded by an Al rich matrix (thus giving rise to the ⟨100⟩ streaks in the X-ray pattern or SAD), and are about 2–10 nm long. The compositions of these zones are still unclear. Experimental work using atomic probe and high-angle annular detector dark-field (HADDF) methods, reported a monolayer composed of Al and Cu (e.g. 25–45 at.-%Cu by Hono *et al.*[81]), one layer of pure Cu zones[79,82] or two layers of pure Cu zones.[83] Recent, tomographic atom probe-field ion microscopy on an Al–1·54 at.-%Cu alloy aged for 30 h at 100°C indicates that while GP1 zones with a Cu concentration of 40% do exist, the vast majority contain more than 65%Cu and half contain about 100%Cu.[84] In a theoretical study, Takeda *et al.*[85] considered the stability of four models of zones containing different solute concentrations using the extended Hueckel molecular orbital method (EHMO). Figure 25 schematically shows the atomic arrangements of the central (001) planes in which the GPI zones are formed with five copper atoms. The calculations based on the EHMO indicated that a GPI zone comprising 40–50 at.-%Cu (i.e. Fig. 25*b* and *c*) is most stable in the energy calculation for an Al–4 at.-%Cu alloy.

In electron diffraction in the TEM, GPI zones cause continuous electron diffraction streaks through {200} type matrix spots parallel to ⟨001⟩ directions as shown in Fig. 26*a*. It should be noted that these streaks are caused by the shape and direction of the zones (plates) rather than by any crystal structure. On further aging the continuous streaks through $\{200\}_{Al}$ [001] SAD pattern may break up and give rise to pronounced maximum intensities at $\{100\}_{Al}$ (Fig. 26*b*),[77,86] thus indicating further evolution of the ordering. This pre-precipitate is generally termed either GPII zone or θ'' phase, but since it has a definite crystal structure, the symbol θ'' is often preferred. Further indications for the existence of a distinct phase is that DSC curves of Al–Cu alloys can show a two-stage dissolution effect before θ' formation occurs.[87] These θ'' precipitates, usually of maximum thickness 10 nm and up to 150 nm diameter, have a tetragonal structure which fits perfectly with the

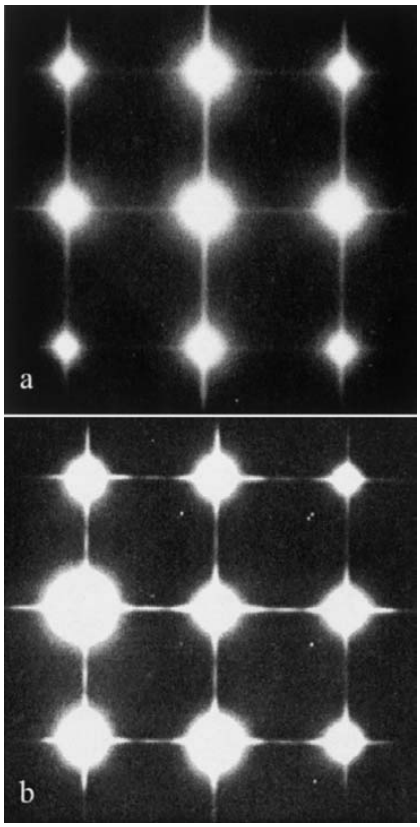

26 $[001]_{Al}$ diffraction patterns in Al–6·2Cu–0·28Mg (wt-%) alloy corresponding to *a* GP (aging at 130°C for 5 h) and *b* θ'' (aging at 130°C for 112·8 h) (by courtesy of Papazian, from Ref. 77)

aluminium unit cell in the *a* and *b* directions but not in the *c* direction. Guinier[88] first detected streaks by XRD and reported the θ'' as tetragonal with $a=0{\cdot}404$ nm and $c=0{\cdot}79$ nm. He postulated that the structure consisted of two pure Cu layers separated by two layers of 1/6 Cu + 5/6 Al and one Al layer to give the same composition as the equilibrium precipitate θ ($CuAl_2$), as shown in Fig. 27*a*. Gerold[89] proposed a θ'' phase consisting of two pure Cu layers separated by three Al layers along ⟨100⟩, in which the surrounded region is strained towards the Cu layers as a result of the smaller size of the Cu atoms ($\gamma_{Cu}=0{\cdot}128$ nm) compared to the Al atoms ($\gamma_{Al}=0{\cdot}143$ nm) as shown in Fig. 27*b* (the unit cell composition in this structure gives Al_3Cu rather than Al_2Cu). Figure 27*c* and *d* shows the simulated diffraction pattern of [001] for the Guinier and Gerold models. Comparison of Fig. 27 with Fig. 26*b* is inconclusive as to which is the more suitable description for θ''. The Gerold model has long been favoured and supported by first principles energy calculations,[23,90,91] some HREM results,[84,92] as well as by recent work using HADDF method which clearly showed the three Al layers sandwiched by single Cu layers.[89] Other HREM experiments[93] provided evidence for structures consisting of two Cu layers separated by a single Al layer as well as other more complex structure types. FIM work by Hirano[94] indicated that θ'' consisted of two Cu rich layers separated by two or three layers of lower Cu content. Wang *et al.*[91] investigated the atomic structures and formation enthalpies of layered Al–Cu superlattices with Cu atoms on 100 planes through first principles PW-PP calculations. The superlattices included the

International Materials Reviews IMR413.3d 22/4/05 21:24:42
The Charlesworth Group, Wakefield +44(0)1924 369598 - Rev 7.51n/W (Jan 20 2003)

S.C. Wang and M.J. Starink, Review of precipitation in Al-Cu-Mg(-Li) alloys, Int Mater Rev., 2005, Vol. 50, pp 193-215

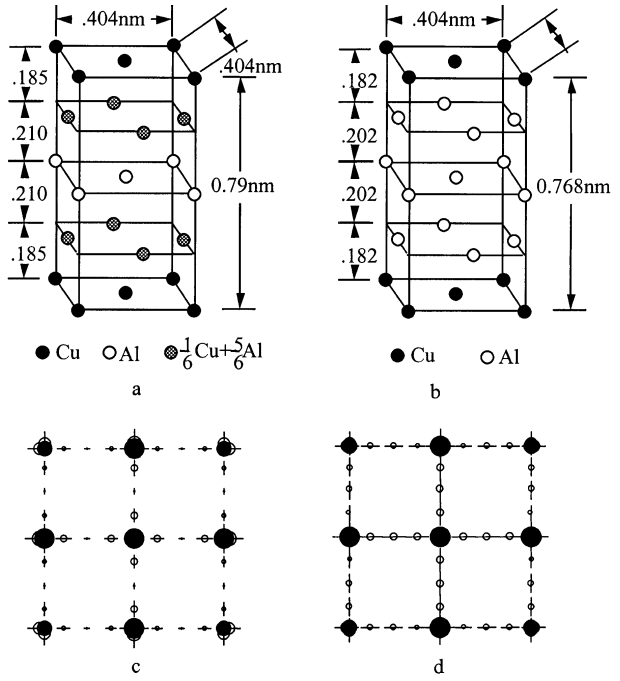

27 *a* Guinier model of GPII/θ" (from Ref. 88); *b* Gerold model of GPII/θ" (from Ref. 89), *c* simulated $[001]_{Al}$ diffraction patterns for Guinier model of GPII/θ" and *d* simulated $[001]_{Al}$ diffraction patterns for Gerold model of GPII/θ"; simulation was carried out with Diffract 1·2a software; sizes represent reflection intensities, and open and full circles correspond to GPII/θ" and Al matrix, respectively

Gerold structure (Al_3Cu) as well as more dilute Al_5Cu, Al_7Cu, Al_9Cu, etc. type structures, and indicated that the supercell formation enthalpy decreases almost linearly with rising Cu content. Of these supercells, the Gerold structure (Al_3Cu) was the most stable.

The GPII/θ" phase as an independent or separate structure to GPI has been questioned by several researchers. Phillips[46] found that HREM showed that the breaking up of the continuous streaks in SAD patterns was not accompanied by any distinct microstructural change and proposed that the transformation from GPI to GPII/θ" is gradual and any distinction based on size is arbitrary. In line with this, Karlik *et al.*[84] observed some structures consisting of a larger Cu layer and a smaller Cu layer separated by three layers of Al, which appear to be the very early stage of GPII formation from a single layer GPI zone. From the investigation of diffuse diffraction of synchrotron radiation, Matsubara and Cohen[79] indicated that the so-called extra reflections in the GPII/θ" state are in fact thickness fringes and the transition between GPI and GPII/θ" was in reality a coarsening reaction.

In attempting to draw general conclusions from the work on GPI and GPII/θ" reviewed in this section, it appears that they can be generalised within two frameworks, one focuses on local atomic scale effects and a second one focuses on the nucleation of θ" (Al_3Cu) phase. Within the framework of atomic interactions, the single layer Cu rich plate termed a GPI zone is considered an important structure. This view is most commonly accepted and in a precipitation sequence one may describe this as

$$SSS \rightarrow GPI(Al_9Cu, Al_7Cu, Al_5Cu, Al_3Cu)$$
$$\rightarrow GPII/\theta''(Al_3Cu) \rightarrow \theta'(Al_4Cu) \rightarrow \theta(Al_2Cu)$$

Here the compositions of zones (Al_9Cu, Al_7Cu, Al_5Cu, Al_3Cu) is given to incorporate the modelling work by Wang *et al.*[91] on the formation enthalpies of layered Al–Cu superlattices, which suggests a process of increasing accumulation of copper atoms by means of local coagulation of Cu platelets.

An alternative framework considers the different stages of the formation of a single metastable structure, the Gerold structure of Al_3Cu (Fig. 27*b*). In the very early stages of Al_3Cu formation, the amount of Cu segregated to each nucleus will be limited and each nucleus will take the form of a layer enriched in Cu, thus forming what may be considered as about four layers of the Al_3Cu structure (or even up to seven layers, with one layer of Cu and up to three layers of Al on each side). Considering the diameter of these thin precipitates reported in the literature (3–10 nm[83,95]), and considering that four atomic layers is about 0·8 nm, the aspect ratio is about 4–12. This is similar to the range of aspect ratios encountered for larger, more fully developed θ" precipitates, and well within the range of aspect ratios of plate shaped and rod shaped semi-coherent phases encountered in Al alloys (e.g. semi-coherent S, θ'). Further growth of these Al_3Cu nuclei will expand beyond the seven layers and thus add layers of Cu. This growth is thus in essence a coarsening reaction, but because the precipitate will add a second layer of Cu, which necessitates substantial additional amounts of Cu diffusing to the growing precipitate, the kinetics of the reaction is likely to be a two-stage one. The transition is a competition between the thermodynamic driving force (favouring multilayers) and interfacial energy around the structure.[90] In this view of the early stages of precipitation in Al–Cu alloys, there is no need for the term GP zone: the single Cu rich layers are simply an early stage of the formation of the metastable Al_3Cu precipitates, and its appearance, at this stage, as single extended layers of Cu is a result of the combination of (i) the structure of the Al_3Cu phase containing layers of Al identical to the matrix thus making that part of the Al_3Cu phase indistinguishable from the matrix, (ii) the limited amount of Cu that will have diffused to the nucleus and (iii) the coherency of the Al_3Cu structure in the direction parallel to the Cu layers. In this present interpretation, the occasional observation of structures consisting of Cu layers separated by one or two layers of Al would be explained as Al_3Cu phase with a stacking fault, which could arise owing to intergrowth of two single layers of Cu nucleated at some distance away from each other. As a result of the similarities in structure on each side of the fault, these stacking faults will have very low energies, and thus their occasional occurrence should come as no surprise. In this framework, the precipitation sequence can be written as

$$SSS \rightarrow \theta''(Al_3Cu) \rightarrow \theta'(Al_2Cu) \rightarrow \theta(Al_2Cu)$$

where the first stage of θ" formation consists of very thin (less than 1 nm) θ" plates of a few atomic layers, which have been indicated as GPI zones.

International Materials Reviews IMR413.3d 22/4/05 21:24:48
The Charlesworth Group, Wakefield +44(0)1924 369598 - Rev 7.51n/W (Jan 20 2003)

S.C. Wang and M.J. Starink, Review of precipitation in Al-Cu-Mg(-Li) alloys, Int Mater Rev., 2005, Vol. 50, pp 193-215

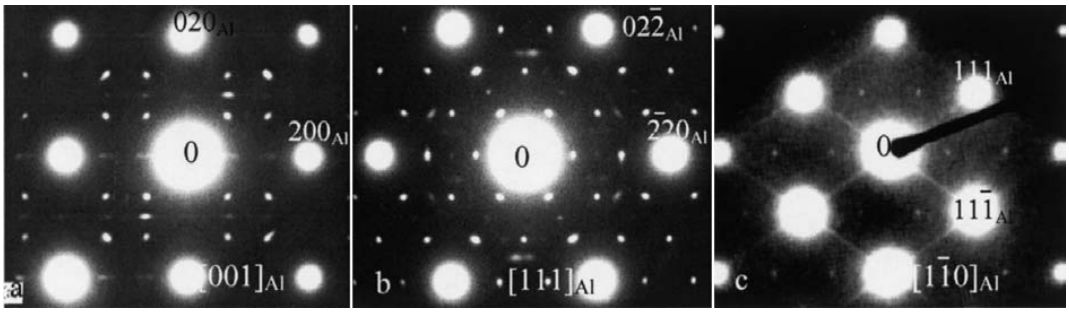

28 Diffraction patterns of Ω phase observed from *a* $[001]_{Al}$ and *b* $[111]_{Al}$ in Al–4 wt-%Cu–0·3 wt-%Mg–0·4 wt-%Ag (by courtesy of Knowles and Stobbs from Ref. 104); and *c* $[1\bar{1}0]_{Al}$ in Al–4·66 wt-%Cu–0·74 wt-%Mg–0·57 wt-%Ag (from Ref. 103) in Al–Cu–Mg–Ag alloys

Precipitation strengthening

Compared to Al–Cu–Mg alloys, recent work on precipitation strengthening in Al–Cu based alloys that are strengthened by precipitates from the θ (Al_2Cu) aging sequence has been very limited. This is mainly because of the limited technological applications for these alloys. It is commonly accepted that in these alloys when aged below the solvus of zones, the first stage of hardening and the plateau in hardness following it are due to the formation of predominantly single layer Cu rich 100 plates, commonly indicated as GPI zones.[96] The formation of θ'' (Al_3Cu) is usually considered to occur in the stage where the hardness increases following the plateau stage.[97] It is mostly accepted that at the peak hardness stage θ' (Al_2Cu) has replaced θ''. θ' is predominantly non-shearable.[94]

Precipitates forming during aging III: the Ω phase

Besides S, GPB2/S'', θ'', θ', θ and σ one further precipitate phase has been reported for Al–Cu–Mg alloys with compositions in the $\alpha+S$ and $\alpha+\theta+S$ phase fields.[98,99] This phase, generally termed the Ω phase, has been extensively studied in Al–Cu–Mg–Ag alloys, and this section will include data on Al–Cu–Mg alloys with Ag addition.

Ω *phase*

Auld[100,101] reported that in an aged Al–2·5Cu–0·5Mg–0·5Ag (wt-%) alloy thin hexagonal-shaped platelike particles of a new phase, designated θ'_M, formed uniformly on the {111} matrix planes at the expense of the tetragonal θ' phase which forms on the $\{001\}_{Al}$ planes. The proposed atomic positions of the phase are shown Table 6. The θ'_M phase described by Auld has the same composition and similar lattice parameters as the θ phase (Al_2Cu). Other authors have observed precipitates that are in many ways similar to θ'_M but generally termed them Ω phase.[102] Ω phase has been argued to be monoclinic,[100,101] hexagonal,[103] orthorhombic[104] and tetragonal.[105] Details of the proposed structures are shown in Table 6.

It is very interesting to investigate whether the observations that led to this multitude of proposed structures can in fact be attributed to one single phase. To compare the reported structures, all were converted to orthorhombic structures as shown in Table 7. All the structures have nearly identical *a* and *b* lattice parameters but *c* is different. As the precipitates are only a few nanometres thick in the $(001)_\Omega$ direction (which is parallel to $\{111\}_{Al}$), the diffraction spots along $\langle 111\rangle_{Al}$ may not be distinguished but instead give rise to streaks. Accordingly, all the structures should in practice give the same diffraction patterns (including double diffractions) in $\langle 001\rangle_{Al}$, $\langle 111\rangle_{Al}$ and $\langle 110\rangle_{Al}$. Simulation of diffraction patterns (not presented) confirmed this and showed that for all reported structures, the patterns were consistent with the experimentally determined patterns in Fig. 28. Figure 29*a* and *b* shows the diffraction patterns of Ω phase in $[112]_{Al}$ by Fonda *et al.*[106] and Kerry and Scott.[103] In fact, Fig. 29*a* can also be obtained by the structures proposed by Auld,[101] Knowles and Stobbs[104] and Garg and Howe.[105] All the above SAD data indicate that the observations which led to the first three crystal structures described in Table 6 were in fact all on one single phase, possibly with very small differences in atomic coordinates.

Table 6 Spaces group and atomic positions of Ω structure reported in the literature

Phase	Structure	Lattice parameter, nm	Multiplicity/Wyckoff letter	Positions *x*	*y*	*z*	Occupancy	Reference
θ'_M	*P112/m* (monoclinic)	*a*=0·496 *b*=0·496 *c*=0·848	2j	0·5	0	0·25	100%Cu	101
			2k	0	0·5	0·25	100%Cu	
			2i	0	0	1/6	100%Al	
			2l	0·5	0·5	1/3	100%Al	
			2m	1/3	2/3	0	100%Al	
			2n	1/6	5/6	0·5	100%Al	
Ω	*Fmmm* (orthorhombic)	*a*=0·496 *b*=0·859 *c*=0·848	8f	0·25	0·25	0·25	100%Cu	104
			8h	0	1/3	0	100%Al	
			8i	0	0	1/6	100%Al	
θ_M	Tetragonal	*a*=0·6066 *c*=0·495	Coordinates similar to θ in Table 5					105
Ω	Hexagonal	*a*=0·496 *c*=0·701	Unknown					103

International Materials Reviews IMR413.3d 22/4/05 21:24:50
The Charlesworth Group, Wakefield +44(0)1924 369598 - Rev 7.51n/W (Jan 20 2003)

S.C. Wang and M.J. Starink, Review of precipitation in Al-Cu-Mg(-Li) alloys, Int Mater Rev., 2005, Vol. 50, pp 193-215

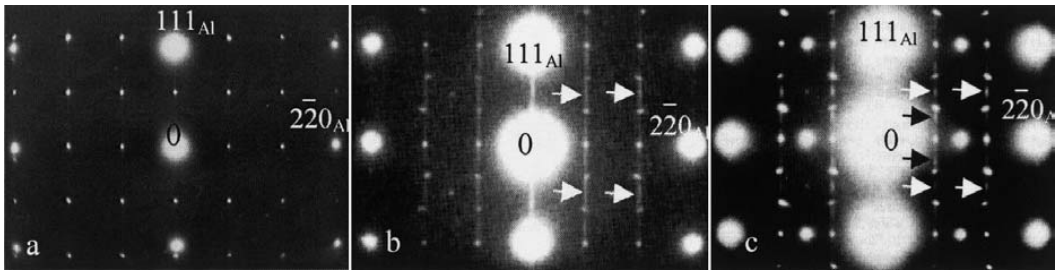

29 $[\bar{1}\bar{1}2]_{Al}$ patterns and reflections from *a* Ω (from Ref. 106); *b* Ω (from Ref. 103) and *c* T_1 (from Ref. 107) (the superlattice spots are caused by δ' phase)

The pattern in Fig. 29*b* is after Kerry and Scott[103] who determined the structure as hexagonal with c=0·701 nm (the fourth structure in Table 4). This pattern cannot be rationalised by the orthorhombic[104] or tetragonal[105] Ω structures, and hence should correspond to a different structure. However, the structure proposed by Kerry and Scott[103] cannot give an explanation for the streaks in the SAD patterns (indicated by arrows in Fig. 29*b*). It is interesting to note that the pattern in Fig. 29*b* is identical to that of T_1 phase (Al_2CuLi, hexagonal structure with a=0·496 nm and c=0·935 nm) except for superlattice spots caused by δ' in Al–Cu–Li alloys as shown in Fig. 29*c*.[107] Therefore, we believe that the c parameter for this phase (Ω), should be the same as the c value in T_1, i.e. it is expected to be 0·935 nm instead of 0·701 nm proposed by Kerry and Scott.[103] This argument is supported by HREM data by Reich *et al.*[108] for an Al–4·3Cu–0·3Mg–0·8Ag (wt-%) alloy aged at 180°C for 5 min and 10 h (a similar aging treatment was applied in the work of Kerry and Scott). As shown in Fig. 30*a*, the c value for the precipitate present after a short aging time (5 min at 180°C) is 0·935 nm, whereas the c value decreased to 0·90 nm after aging for 10 h at 180°C (analysis of published HREM micrographs by the present authors). The simulation of $[310]_\Omega$ by the present authors (insert in Fig. 30*b*) fits well with the HREM image using the same atom coordinates as the orthorhombic Ω structure[104] with c modified to be 0·90 nm. An analysis of HREM pictures of Reich *et al.*[108] (performed by the present authors) suggests that the c value of Ω is variable and on aging it changes until a value of 0·848 nm is reached. This argument is supported by two further observations. First, Fonda *et al.*[106] found that the c lattice parameter of Ω is between 0·848 nm (Knowles and Stobbs[104]) and 0·858 nm (Garg and Howe[105]) in an Al–5Cu–0·5Mg–0·5Ag (wt-%) alloy. And the obtained CBED pattern[106] was distorted less than 0·05% from a fourfold symmetry, compared with a distortion of 1·3% predicted for the orthorhombic structure of Knowles and Stobbs,[104] i.e. the c value is 0·8576 nm for Ω after aging at 375°C for 1 h.[106] Second, in recent HREM findings, Yoshimura

Table 7 Proposed structures for Ω phase and corresponding orthorhombic structures (converted by present authors)

Phase	Phase structure and O.R. with matrix	Converted orthorhombic structure and O.R. with matrix	Composition (wt-%)/aging
	Monoclinic, $a=b$=0·496 nm, c=0·848 nm, γ=120°, *P2/m* $[\bar{1}\bar{1}20]_\Omega//[\bar{1}\bar{1}2]_{Al}$, $[1\bar{1}00]_\Omega//[1\bar{1}0]_{Al}$, $[0001]_\Omega//[111]_{Al}$	a=0·496 nm, b=0·859 nm, c=0·848 nm $[100]_O//[\bar{1}\bar{1}2]_{Al}$, $[010]_O//[1\bar{1}0]_{Al}$, $[001]_O//[111]_{Al}$	Al–2·5Cu–0·5Mg–0·5Ag 200°C/288 h[100,101]
	Hexagonal, a=0·496 nm, c=0·701 nm $[\bar{1}\bar{1}20]_\Omega//[\bar{1}\bar{1}2]_{Al}$, $[1\bar{1}00]_\Omega//[1\bar{1}0]_{Al}$, $[0001]_\Omega//[111]_{Al}$	a=0·496 nm, b=0·859 nm, c=0·701 nm $[100]_O//[\bar{1}\bar{1}2]_{Al}$, $[010]_O//[1\bar{1}0]_{Al}$, $[001]_O//[111]_{Al}$	Al–4·7Cu–0·7Mg–0·6Ag 170°C/2 h[103]
Ω	Orthorhombic, space group is *Fmmm*, a=0·496 nm, b=0·859 nm, c=0·848 nm (=Knowles & Stobbs'[104] structure) $[100]_\Omega//[\bar{1}\bar{1}2]_{Al}$, $[010]_\Omega//[1\bar{1}0]_{Al}$, $[001]_\Omega//[111]_{Al}$	a=0·496 nm, b=0·859 nm, c=0·848 nm (=Knowles & Stobbs'[104] structure) $[100]_O//[\bar{1}\bar{1}2]_{Al}$, $[010]_O//[1\bar{1}0]_{Al}$, $[001]_O//[111]_{Al}$	Al–4Cu–0·3Mg–0·4Ag 167°C/24 h[104] Al–4Cu–0·3Mg–0·4Ag 200°C/100 h[76]
	As Knowles & Stobbs'[104] structure above except c=0·8576 nm	As Knowles & Stobbs'[104] structure above except c=0·8576 nm	Al–4·3Cu–0·3Mg–0·8Ag 375°C/1 h[106]
	As Knowles & Stobbs'[104] structure above except c=0·935 nm*	As Knowles & Stobbs'[104] structure above except c=0·935 nm*	Al–5Cu–0·5Mg–0·5Ag 180°C/5 min[108]
	As Knowles & Stobbs'[104] structure above except c=0·90 nm*	As Knowles & Stobbs'[104] structure above except c=0·90 nm*	Al–5Cu–0·5Mg–0·5Ag 180°C/10 h[108]
	As Knowles & Stobbs'[104] structure above except c=0·87–0·90 nm	As Knowles & Stobbs'[104] structure above except c=0·87–0·90 nm	Al–3·2Cu–1·6Li 220°C/11d[109]
	Tetragonal, $a=b$=0·6066 nm, c=0·496 nm $[001]_\Omega//[\bar{1}\bar{1}2]_{Al}$, $[110]_\Omega//[1\bar{1}0]_{Al}$, $[\bar{1}10]_\Omega//[111]_{Al}$	a=0·496 nm, b=0·858 nm, c=0·858 nm $[100]_O//[\bar{1}\bar{1}2]_{Al}$, $[010]_O//[1\bar{1}0]_{Al}$, $[001]_O//[111]_{Al}$	Al–5Cu–0·5Mg–0·5Ag 250°C/300 h[105]
θ	Tetragonal, space group is *I4/mcm*, $a=b$=0·6066 nm, c=0·4874 nm, Vaughan II O.R. is $[001]_\theta//[\bar{1}\bar{1}2]_{Al}$, $[110]_\theta//[1\bar{1}0]_{Al}$, $[\bar{1}10]_\theta//[111]_{Al}$	a=0·4874 nm, b=0·858 nm, c=0·858 nm $[100]_O//[\bar{1}\bar{1}2]_{Al}$, $[010]_O//[1\bar{1}0]_{Al}$, $[001]_O//[111]_{Al}$	Al–4Cu 350°C/15 min 400°C/5 min[110]
T_1	Hexagonal, space group is *P6/mmm* a=0·496 nm, c=0·935 nm $[\bar{1}\bar{1}20]_{T1}//[\bar{1}\bar{1}2]_{Al}$, $[1\bar{1}00]_{T1}//[1\bar{1}0]_{Al}$, $[0001]_{T1}//[111]_{Al}$	a=0·496 nm, b=0·859 nm, c=0·935 nm $[100]_O//[\bar{1}\bar{1}2]_{Al}$, $[010]_O//[1\bar{1}0]_{Al}$, $[001]_O//[111]_{Al}$	Al–2·85Cu–2·3Li–0·12Zr 190°C/132 h[107]

*Calculated by the present authors from HREM micrographs presented in Ref. 108 (Fig. 30).

International Materials Reviews IMR413.3d 22/4/05 21:24:51
The Charlesworth Group, Wakefield +44(0)1924 369598 - Rev 7.51n/W (Jan 20 2003)

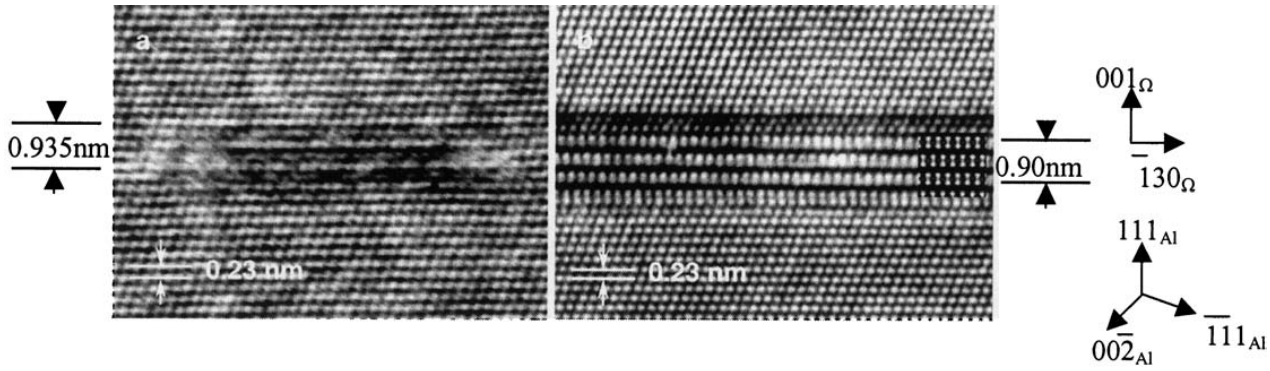

30 [1$\bar{1}$0] HREM image of typical precipitates in Al–4·3Cu–0·3Mg–0·8Ag (wt-%) alloy aged at 180°C for *a* 5 min and *b* 10 h (by courtesy of Reich, from Ref. 108)

et al.[109] confirmed the existence of Ω phase with the *c* value ranging between 0·87 and 0·90 nm in Al–3·2Cu–1·6Li (wt-%). The reason for the variable *c* value of Ω phase is not clear; it may be as a result of the aging temperature/time (as was noted in Table 7, in general the higher *c*, the lower aging temperature/time) or compositions such as addition of Li.[109] It has been shown that θ phase forms initially on $\{111\}_{Al}$ with c=0·935 nm (perfect matching) on aging at 180°C for 5 min and then the *c* lattice parameter changes to 0·90 nm on aging at 180°C for 10 h.[104] Considering the new evidence for variable *c* value of Ω phase, the Ω phase is probably an orthorhombic structure with the *c* value ranging from 0·935 nm to an equilibrium value at 0·848 nm. The tetragonal structure proposed by Garg and Howe[105] is perhaps related to the case where the *c* value happens to be close to 0·858 nm (Table 7) which corresponds to the distorted θ structure.

The similarities between the Ω and θ phases have been mentioned by several authors. For example, Auld[100] noticed that the Ω phase (θ'_M) might be formed through very small atom movements from equilibrium θ phase. In the work by Garg and Howe,[105] the point group of Ω phase (θ_M) has been determined as *4/mmm* by CBED, which is the same point group as the θ phase. Garg and Howe[105] suggested Ω phase to be a distorted form of the θ phase, i.e. the *c*-parameter increases 1·76% to achieve perfect atomic matching on the $\{111\}_{Al}$ planes. It has been noted,[104] that the orientation relationship of Ω with the matrix is consistent with one of the 22 orientation relationships of the tetragonal θ phase (the orientation referred to as 'Vaughan II'[110]). It is thought that this selection of orientation relationship is because of the addition of Ag. Specifically, Ag has been suggested to reduce the stacking fault energy on {111} planes,[103] which indeed would stimulate the orientation relationships observation. In fact, if the Ω coordinates are converted to an *I4/mcm* tetragonal structure, as shown in Table 8, the atomic positions of Ω and θ are found to be extremely close. The largest atomic displacement between two structures is only 0·86%.

Table 8 Atomic positions of Ω[104] and θ[71] based on *I4/mcm* structure

Atom	Multiplicity Wyckoff letter	Coordinate (*x*, *y*, *z*) Ω	θ
Cu	4a	(0 0 0·25)	(0 0 0·25)
Al	8h	(0·1667 0·6667 0)	(0·1581 0·6581 0)

Interestingly, besides S (Al_2CuMg) precipitates in 2124 alloy (without addition of silver), Jin and co-workers[111,112] found diffraction spots similar to Ω phase on one-third or two-thirds of $\{220\}_{Al}$ but these authors designated these spots as due to X phase. The X phase was suggested as orthorhombic crystal structure (*Cmmm*) with a=0·492 nm, b=0·852 nm and c=0·701 nm. Note that the atomic arrangement in the suggested orthorhombic crystal structure is unlikely, as the spacing between two Mg atoms in this model is 0·246 nm compared to the atomic diameter of Mg of 0·320 nm. A possible explanation of the patterns is that they are caused by Ω phase.

Precursor to Ω phase

Based on their TEM observations, Abis *et al.*[113] proposed a new precursor phase which was stable to 190°C and designated it as Ω' phase. It has a hexagonal crystal structure based on the $MgZn_2$ prototype (space group $P6_3/mmc$) with lattice parameters a=0·507 nm and c=0·692 nm. However, this idea was not supported by other research. For example, Ringer *et al.*[39] ruled out the possibility of the existence of such a precursor phase based on their HREM results.

Addition of trace elements Ag and Mg to Al–Cu/Al–Cu–Mg alloys may change the precipitation sequence from θ/S to Ω. Taylor *et al.*[114] proposed that Ag and Mg form Mg_3Ag (possible hexagonal structure with a=0·487 and c=0·777 nm) which then acts as nuclei for Ω precipitation. However, X-ray investigations of the Al–Ag–Mg ternary alloys have failed to isolate Mg_3Ag particles even at high Mg/Ag ratios, and instead the compound MgAg (B2 structure, a=0·330 nm) was identified.[115] Furthermore, Lim *et al.*[116] theoretically evaluated Gibbs free energies of several intermetallic phases in Al–Cu–Mg–Ag alloys, and showed that the intermetallic compound Mg_3Ag cannot exist under the conditions of Ω precipitation. APFIM and 3DAP also found evidence of Ag–Mg clusters, rather than the $AgMg_3$ phase, in Al–Cu–Mg–Ag during the early stages of aging after quenching.[39,108] Subsequently, Cu atoms will segregate into the clusters whereas Ag and Mg will disperse. Taken together, these results show that a small amount of Mg is essential for precipitation of Ω phase and that Ag serves to stimulate precipitation of Ω[117,118] even though arguments exist regarding the Ag and Mg segregation on the interface of Ω and Al.[74,119,120]

S.C. Wang and M.J. Starink, Review of precipitation in Al-Cu-Mg(-Li) alloys, Int Mater Rev., 2005, Vol. 50, pp 193-215

Al–Cu–Mg–Li alloys

Constituent phases

The presence of Li in Al–Cu–Mg alloys can cause a range of very complex intermetallic phases, which are listed in Table 9. After liquid–solid reactions (i.e. in an ingot), eutectic icosahedral phases T_2 or C phase have been found to be the dominant phases in the eutectic structures of the as cast 8090 alloys [Cu/Mg (wt-%)=1·39][121] and an alloy with a lower Cu/Mg ratio (0·88).[122] R phase was also reported to form during casting.[123] More stable intermetallics may form by solid–solid reactions during subsequent heat treatments such as homogenisation, solution treatment and aging. T_2 phase was found to be stable up to ~420°C whereas R remained present up to ~560°C in the 8090 alloy.[121] T_2 phase may re-form during aging of 8090 type alloys, initially mainly on high-angle grain boundaries (HAGBs) and later in the matrix, with smaller size than in the as cast materials.[124] The tetragonal C phase, too, can be present as a major phase in the as cast materials, and dissolves during homogenisation and precipitates in a modified form (reduced c parameter) during subsequent annealing.[122] C and T_2 formation by solid–solid reaction occurs competitively depending on the Cu/Mg ratio. For example, the microstructure was dominated by T_2 with Cu/Mg=1·7,[124] by C with Cu/Mg=0·88,[122] and with comparable amounts of the two phases present in an alloy with Cu/Mg=1·3.[125]

As presented in several publications, many of the phases in Table 9 have similar compositions and may transform from one to another.[126–132] For instance, T2 may transform to R phase via O phase[121] or C phase[131] during heat treatment. These intermetallic phases are generally thought to be detrimental to the properties of Li containing alloys (e.g. T_2 is detrimental to toughness), but in view of the multitude of phases that can be present, more work is needed in this area to further understand the formation of intermetallics in Al–Cu–Li–Mg alloys, and the influence these phases have on the properties.

Dispersoids

Grain structure control in Al–Cu–Mg–Li alloys is generally achieved by addition of Zr. Dispersoids formed are $L1_2$ ordered β' (Al_3Zr), and they form during homogenisation of cast alloys from the supersaturated solid solution. They are very stable as a result of low Zr solubility in Al, small misfit and sluggish diffusion of Zr in Al. Consequently, these precipitates are very effective in pinning grain and subgrain boundaries during thermal and mechanical processing of Al alloys of commercial interest.[133] The dispersoids improve the mechanical properties by retarding recrystallisation and suppressing grain growth, and by reducing the inhomogeneous distribution of slip caused by the presence of shearable precipitates.[134] Furthermore, as the lattice parameter of Al_3Zr is slightly larger than Al whereas that of Al_3Li is less, coherent Al_3Zr precipitates provide heterogeneous nucleation sites for the major strengthening phase Al_3Li as these complexes will relieve the misfit strain as well as interfacial energy.[135]

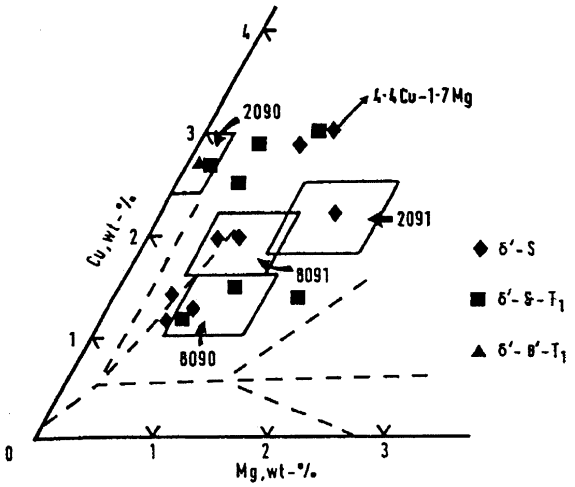

31 Precipitate phases reported in Al–Cu–Mg–(Li) alloys on aging at 190°C; compositions of alloys are shown in Table 1 (from Ref. 137)

Precipitates forming during aging: T_1 phase and δ' phase

Considerable effort has gone into the development of Al–Cu–Mg–Li alloys, as a result of their potential for use as high-strength aerospace alloys, with density lower than other high strength Al based alloys. Usually up to three precipitation sequences occur during aging of any one alloy. These sequences include (1) the formation of spherically shaped $L1_2$ ordered δ' phase (Al_3Li), (2) the S (Al_2CuMg) sequence, (3) the θ (Al_2Cu) sequence, and (4) a sequence leading to the plate shaped T_1 phase (Al_2CuLi).[136] Figure 31 shows the expected precipitation sequences in different alloys in the form of a section through the phase diagram[137] (see Table 1 for compositions).

The crystal structure of the δ' phase is well established with space group $Pm\bar{3}m$ and lattice parameter a=0·405 nm. The δ' phase may form coherently as shells around the β' (Al_3Zr) dispersoid particles. The δ' phase is fully coherent with the matrix: $(100)_{\delta'}//(100)_{Al}$, $[001]_{\delta'}//[001]_{Al}$. On continued aging, the δ' phase will eventually be replaced by stable intermetallics such as the δ (AlLi) or T_2 phases. However, owing to its full coherency with the matrix, δ' phase is relatively stable and on typical isothermal aging treatments below its

Table 9 Intermetallic phases reported in Al–Li–Cu–Mg alloys

T_2-$Al_5Cu(Li,Mg)_3$	Icosahedral, point group $m\bar{3}\bar{5}$	Nucleated on HAGB
Z-$Al_6Cu(Li,Mg)_3$	$P6_3/mmc$, a=1·403 nm, c=2·8 nm	127
C-$Al_6Cu(Li,Mg)_3$	Tetragonal, $P4_2/mmc$, a=1·4 nm, c=5·41–6·0 nm (~4a)	122, 123
τ-$Al_6(Cu,Zn)Li_3$	$P4_2/mmc$, a=1·39 nm, c=8·245 nm (~6a)	123
O-$Al_6Cu(Li,Mg)_3$	Orthorhombic, a=1·35 nm, b=1·38 nm (~a), c=16·22 nm (~12a)	121, 128
R-$Al_5Cu(Li,Mg)_3$	$Im\bar{3}$, CaF_2 prototype, a=1·39 nm	129
R'-$Al_5Cu(Li,Mg)_3$	$Pm\bar{3}n$, a=1·39 nm	130
Y-$Al_5Cu(Li,Mg)_3$	fcc, a=2 nm	131
δ-AlLi	NaTl prototype, a=0·637 nm	132
T-Al_2LiMg	$Fd\bar{3}m$, a=2·058 nm	127

International Materials Reviews IMR413.3d 22/4/05 21:24:58
The Charlesworth Group, Wakefield +44(0)1924 369598 - Rev 7.51n/W (Jan 20 2003)

S.C. Wang and M.J. Starink, Review of precipitation in Al-Cu-Mg(-Li) alloys, Int Mater Rev., 2005, Vol. 50, pp 193-215

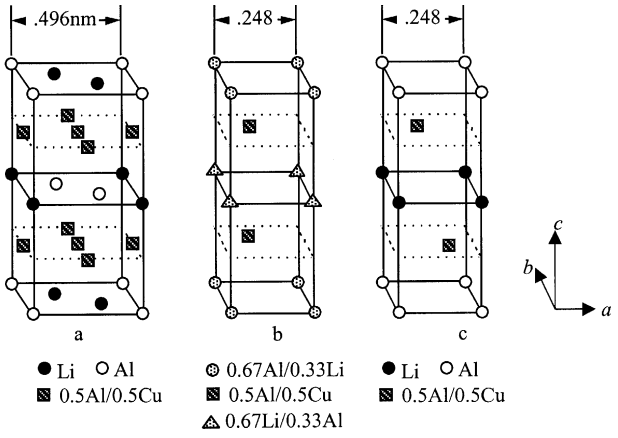

32 Models proposed for T_1 structure by *a* Huang and Ardell (from Ref. 107), with space group *P6/mmm* and lattice parameters *a*=0·496 nm, *c*=0·935 nm; *b* Cassada *et al.* (from Ref. 140), with space group *P$\bar{6}$m2* and lattice parameters *a*=0·248 nm, *c*=0·935 nm; *c* Howe *et al.* (from Ref. 141), with space group *P$\bar{3}$m1* and lattice parameters *a*=0·248 nm, *c*=0·935 nm

metastable solvus, dissolution of δ' phase generally only occurs around grain boundaries and other interfaces, where stable phases like δ (AlLi) and T_2 nucleate.

The S and θ sequences have been discussed in the above sections, and in this chapter, the T_1 phase will be reviewed. T_1 phase is known to precipitate heterogeneously on dislocations and grain boundaries in Al–Cu–Li based 2090 alloys. Addition of Mg promotes a uniform dispersion of the T_1 plates in the matrix.[138] The T_1 phase was first identified by XRD in the Al–Li–Cu system by Hardy and Silcock.[139] They indicated its crystal system is hexagonal with a=0·496 nm and c=0·935 nm. The orientation relationship with matrix was determined as $(0001)_{T1}//(111)_{Al}$, $[1\bar{1}00]_{T1}//[1\bar{1}0]_{Al}$. The space group was not determined unambiguously, and they suggested that its structure might belong to one of *P622*, *P6mm*, *P$\bar{6}$m2*, or *P6/mmm* space groups. Huang and Ardell[107] proposed its structure to be *P6/mmm* (Table 10 and Fig. 32*a*), and this structure would produce XRD peaks with intensities in fair agreement with those reported by Hardy and Silcock.[139] The *P6/mmm* structure also provides correct predictions for electron diffraction patterns for the zone axes ⟨001⟩, ⟨110⟩, ⟨111⟩, ⟨112⟩, ⟨013⟩ and ⟨114⟩. In contrast, based on their HREM images and simulations, Cassada *et al.*,[140] Howe *et al.*[141] and Herring *et al.*[142] proposed another structure for this phase as shown in Table 10 and Fig. 32*b* and *c*. The two structures have identical orientation relationships with the matrix. The challenge in distinguishing the two structures is that they predict the same diffraction patterns in zone axes ⟨001⟩, ⟨110⟩ and perhaps ⟨112⟩ because of double diffractions. As the proposed structures have different point groups (as well as space groups), the CBED technique may be useful to determine the structure. Indeed, later work on CBED by Vecchio and Williams[143] determined the structure of T_1 to be hexagonal, possessing a *6/mmm* point group and *P6/mmm* space group. The atomic coordinates in the *P6/mmm* space group of T_1 structure have been further refined (Table 10) based on recent single-crystal X-ray diffraction data.[144] However, no more research supports this model.

Rioja and Ludwiczak[145] have suggested that a T_1' phase may form before the precipitation of T_1. To interpret the extra reflections at the positions $\frac{1}{3}\{311\}_{Al}$ and $\frac{2}{3}\{311\}_{Al}$ in $\langle 112\rangle_{Al}$ zones which Rioja and Ludwiczak[145] were unable to index with T_1 proposed by Hardy and Silcock,[139] they proposed T_1' as orthorhombic (Pt_2Mo type) with a=0·2876 nm, b=0·86 nm, c=0·406 nm. This argument, however, was rejected by Huang and Ardell[146] and Cassada *et al.*[147] who pointed out that these extra reflections were caused by extension of reciprocal lattice points in the $[0001]_{T1}$ direction because of the thinness of the T_1 plates or by double diffractions.[148]

In conclusion, the Huang and Ardell[107] model for T_1 phase is commonly accepted. Other proposed structures are perhaps because of the T_1 phase forming by the dissociation of $\frac{1}{2}\langle 110\rangle$ dislocations into $1/6\langle 211\rangle$ Shockley partials bounding a region of intrinsic stacking fault, in which copper and lithium enrichment of the fault produces a thin layer of the T_1 phase.[149]

Table 10 Space groups and atomic positions of T_1 structure reported in literature

Structure	Lattice parameter, nm	Multiplicity/Wyckoff letter	Positions			Occupancy	Reference
			x	*y*	*z*		
P6/mmm (hexagonal)	*a*=0·496 *c*=0·935	1a	0	0	0	100%Al	107, 142
		1b	0	0	0·5	100%Li	
		2c	1/3	2/3	0	100%Li	
		2d	1/3	2/3	0·5	100%Al	
		6i	0·5	0	0·25	50%Al/50%Cu	
P$\bar{6}$m2 (hexagonal)	*a*=0·248 *c*=0·935	1a	0	0	0	67%Al/33%Li	140, 142
		1b	0	0	0·5	67%Li/33%Al	
		2i	2/3	1/3	0·25	50%Al/50%Cu	
P$\bar{3}$m1 (trigonal)	*a*=0·248 *c*=0·935	1a	0	0	0	100%Al	141, 142
		1b	0	0	0·5	100%Li	
		2d	1/3	2/3	0·25	50%Al/50%Cu	
P6/mmm (hexagonal)	*a*=0·495 *c*=0·933	2c	1/3	2/3	0	100%Al	144
		2d	1/3	2/3	0·5	100%Li	
		2e	0	0	0·3569	100%Al	
		2e	0	0	0·0519	66·6%Li	
		6i	0·5	0	0·2363	44·4%Al	
		6i	0·5	0	0·2363	55·6%Cu	

International Materials Reviews IMR413.3d 22/4/05 21:24:59
The Charlesworth Group, Wakefield +44(0)1924 369598 - Rev 7.51n/W (Jan 20 2003)

S.C. Wang and M.J. Starink, Review of precipitation in Al-Cu-Mg(-Li) alloys, Int Mater Rev., 2005, Vol. 50, pp 193-215

References

1. P. Villars, A. Prince and H. Okamoto: 'Handbook of ternary alloy phase diagrams'; 1994, Materials Park, OH, ASM International.
2. E. A. Starke and J. T. Staley: *Prog. Aerospace Sci.*, 1996, **32**, 131–172.
3. R. B. C. Cayless: in 'Metals handbook', Vol. 2, 10th edn, 15–30, Materials Park, OH, ASM International.
4. J. T. Staley: Proc. 3rd Int. Conf. on 'Aluminium alloys (ICAA3)', (ed. L. Arnberg, O. Lohne, E. Nes and N. Ryum), Norwegian Institute of Technology, Trondheim, Norway, June 1992, 107–143.
5. S. C. Wang, C. Z. Li and M. G. Yan: *Chin. J. Aero. Mater.*, 1989, **9**, 39–47 (in Chinese).
6. S. C. Wang, C. Z. Li and M. G. Yan: *Acta Metall. Sinica*, 1990, **3A**, 104–109.
7. J. C. Williams and E. A. Starke: *Acta Mater.*, 2003, **51**, 5775–5799.
8. T. S. Srivatsan, D. Kolar and P. Magnusen: *Mater. Design*, 2002, **23**, 129–139.
9. F. Bergner, G. Zouhar and G. Tempus: *Int. J. Fatigue*, 2001, **23**, 383–394.
10. K. Robinson: *Philos. Mag.*, 1952, **43**, 775–782.
11. L. F. Mondolfo: 'Aluminum alloys – structure and properties'; 1976, London, Butterworths and Co.
12. S. C. Wang, C. Z. Li and M. G. Yan: *Mater. Res. Bull.*, 1989, **24**, 1267–1270.
13. C. Z. Li, S. C. Wang and Y. Jin: Proc. 2nd Int. Conf. on 'Aluminium alloys (ICAA2)', (ed. C. Q. Chen and E. A. Starke, Jr), October, 1990, Beijing, China, 504–507.
14. C. Z. Li, S. C. Wang and M. G. Yan: *Acta Metall. Sinica*, 1992, **5A**, 227–230.
15. Y. A. Bagaryatshy: *Dokl. Akad. S.S.S.R.*, 1952, **87**, 397–401 & 559–562.
16. J. M. Silcock: *J. Inst. Met.*, 1960–61, **89**, 203–210.
17. H. Perlitz and A. Westgren: *Arkiv. Kemi. Mineral. Geol.*, 1943, **16B**, No. 13.
18. 'Pearson's handbook of crystallographic data for intermetallic phases', 2nd edn, (ed. P. Villars); 1991, Materials Park, OH, ASM International.
19. Y. Jin, C. Z. Li and M. G. Yan: *J. Mater. Sci. Lett.*, 1990, **9**, 421–424.
20. M. A. Al-Khafaji, W. M. Rainforth, L. M. Rylands and H. Jones: in 'Electron microscopy and analysis 1999', Institute of Physics Conference Series Number 161, (ed. C. J. Kiely), University of Sheffield, Sheffield, UK, August 1999, 279–282.
21. V. Radmilovic, R. Kilaas, U. Dahmen and G. J. Shiflet: *Acta Mater.*, 1999, **47**, 3987–3997.
22. R. Kilaas and V. Radmilovic: *Ultramicroscopy*, 2001, **88**, 63–72.
23. C. Wolverton: *Acta Mater.*, 2001, **49**, 3129–3142.
24. C. Li and M. Yan: *Mater. Sci. Eng.*, 1983, **57**, 143–147.
25. A. K. Gupta, P. Gaunt and M. C. Chaturvedi: *Philos. Mag. A*, 1987, **55**, 375–387.
26. C. B. Zhang, W. Sun and H. Q. Ye: *Philos. Mag. Lett.*, 1989, **59**, 265–271.
27. J. M. Cowley: 'Diffraction physics', 3rd edn; 1995, Oxford, Elsevier Science.
28. P. Ratchev, B. Verlinden, P. De Smet and P. Van Houtte: *Acta Mater.*, 1998, **46**, 3523–3533.
29. S. P. Ringer, T. Sakurai and I. J. Polmear: *Acta Mater.*, 1997, **45**, 3731–3744.
30. N. Gao, L. Davin, S. C. Wang, A. Cerezo and M. J. Starink: *Mater. Sci. Forum*, 2002, **396–402**, 923–928.
31. M. J. Starink, N. Gao and J. Yan: *Mater. Sci. Eng. A*, 2004, **387–389**, 222–226.
32. A. A. Alekseev, V. N. Anan'ev, L. B. Ber and E. Ya. Kaputkin: *Phys. Met. Metall.*, 1993, **75**, 279–285.
33. T. V. Shchegoleva and N. N. Buinov: *Sov. Phys. Crystallogr.*, 1967, **12**, 552–555.
34. F. Cuisiat, P. Duval and R. Graf: *Scripta Metall.*, 1984, **18**, 1051–1056.
35. H. Shih, N. Ho and J. C. Huang: *Metall. Mater. Trans. A*, 1996, **27**, 2479–2494.
36. A. Charai, T. Walther, C. Alfonso, A. M. Zahra and C. Y. Zahra: *Acta Mater.*, 2000, **48**, 2751–2764.
37. A. M. Zahra, C. Y. Zahra, C. Alfonso and A. Charai: *Scripta Mater.*, 1998, **39**, 1553–1558.
38. R. N. Wilson and P. G. Partridge: *Acta Metall.*, 1965, **13**, 1321–1327.
39. S. P. Ringer, K. Hono, I. J. Polmear and T. Sakurai: *Acta Mater.*, 1996, **44**, 1883–1898.
40. S. P. Ringer, S. K. Caraher and I. J. Polmear: *Scripta Mater.*, 1998, **39**, 1559–1567.
41. S. C. Wang and M. J. Starink: in 'Electron microscopy and analysis 2003', (ed. S. McVitie and D. McComb), Institute of Physics Conference Series Number 179, University of Oxford, Oxford, UK, September 2003, 277–280.
42. S. C. Wang and M. J. Starink: *Mater. Sci. Eng. A*, 2004, **386**, 156–163.
43. A. M. Zahra and C. Y. Zahra: J. Thermal Anal., 1990, **36**, 1465–1470.
44. S. C. Wang, N. Gao and M. J. Starink: unpublished work, University of Southampton, 2003.
45. P. Ratchev, B. Verlinden, P. de Smet and P. van Houtte: *Scripta Mater.*, 1998, **38**, 1195–1201.
46. V. A. Phillips: *Acta Metall.*, 1975, **23**, 751–767.
47. J. K. Park and A. J. Ardell: *Metall. Trans.*, 1983, **14A**, 1957–1965.
48. L. Kovarik, P. I. Gouma, C. Kisielowski, S. A. Court and M. J. Mills: *Mater. Sci. Eng. A*, 2004, **387–389**, 326–330.
49. L. Kovarik, P. I. Gouma, C. Kisielowski, S. A. Court and M. J. Mills: *Acta Mater.*, 2004, **52**, 2509–2520.
50. H. K. Cho: *J. Korean Inst. Met.*, 1976, **10**, 369.
51. A. K. Gupta, A. K. Jena and M. C. Chaturvedi: *Scripta Metall.*, 1988, **22**, 369–371.
52. A. K. Jena, A. K. Gupta and M. C. Chaturvedi: *Acta Metall.*, 1989, **37**, 885–895.
53. V. Gerold and H. Haberkorn: *Z. Metallkd.*, 1959, **50**, 568–574.
54. T. Takahashi and T. Sato: *J. Jpn Inst. Light Met.*, 1985, **35**, 41.
55. Y. Nagai, M. Murayama, Z. Tang, T. Nonaka, K. Hono and M. Hasegawa: *Acta Mater.*, 2001, **49**, 913–920.
56. M. J. Starink: *Int. Mater. Rev.*, 2004, **49**, 191–226.
57. N. Sen and D. R. F. West: *J. Inst. Met.*, 1969, **97**, 87–92.
58. J. T. Vietz and I. J. Polmear: *J. Inst. Met.*, 1966, **94**, 410–419.
59. A. Somoza, A. Dupasquier, I. J. Polmear, P. Folegati and R. Ferragut: *Phys. Rev. B*, 2000, **61**, 14454–14463.
60. L. Reich, S. P. Ringer and K. Hono: *Philos. Mag. Lett.*, 1999, **79**, 639–648.
61. K. Hono: *Prog. Mater. Sci.*, 2002, **47**, 621–729.
62. S. P. Ringer and K. Hono: *Mater. Character.*, 2000, **44**, 101–131.
63. M. J. Starink and J. Yan: Proc. ASM Materials Solutions Conf. 2003, 1st Int. Symp. on 'Metallurgical modeling for aluminum alloys', (ed. M. Tiryakioglu and L. A. Lalli), Pittsburgh, PA, USA, October 2003, ASM International, Materials Park, OH, USA, 119–126.
64. S. Samson: *Acta Chem. Scand.*, 1949, **3**, 809–834.
65. R. D. Schueller, A. K. Sachdev and F. E. Wawner: *Scripta Metall. Mater.*, 1992, **27**, 1289–1294.
66. A. K. Mukhopadhyay: *Metall. Mater. Trans. A*, 2002, **34**, 3635–3647.
67. Q. Li and F. E. Wawner: *J. Mater. Sci.*, 1997, **32**, 5363–5370.
68. R. N. Lumley and I. J. Polmear: *Scripta Mater.*, 2004, **50**, 1227–1231.
69. S. C. Barr, L. M. Rylands, H. Jones and W. M. Rainforth: *Mater. Sci. Technol.*, 1997, **13**, 655–659.
70. A. Guinier: *Solid State Phys.*, 1959, **9**, 293–398.
71. A. Meetsma, J. L. deBoer and S. van Smaalen: *J. Solid State Chem.*, 1989, **83**, 370–372.
72. R. Bonnet: *Acta Crystallogr.*, 1980, **36A**, 116–122.
73. J. M. Silcock, T. J. Heal and H. K. Hardy: *J. Inst. Met.*, 1953–54, **82**, 239–248.
74. G. Wassermann and J. Weerts: *Metallwirtschaft*, 1935, **14**, 605.
75. G. C. Preston: *Philos. Mag.*, 1938, **26**, 855–871.
76. B. C. Muddle and I. J. Polmear: *Acta Metall. Mater.*, 1989, **37**, 777–789.
77. J. M. Papazian: *Metall. Trans.*, 1981, **12A**, 269–280.
78. A. Guinier: *Ann. Phys. Paris*, 1939, **12**, 161–237.
79. E. Matsubara and J. B. Cohen: *Acta Metall.*, 1985, **33**, 1945–1969.
80. T. Sato: *Mater. Sci. Forum*, 2000, **331–337**, 85–96.
81. K. Hono, T. Hashizume, Y. Hasegawa, K. Hirano and T. Sakurai: *Scripta Metall.*, 1986, **20**, 487–492.
82. V. Gerold: *Scripta Metall.*, 1988, **22**, 927–932.
83. T. J. Konno, K. Hiraga and M. Kawasaki: *Scripta Mater.*, 2001, **44**, 2303–2307.
84. M. Karlik, A. Bigot, B. Jouffrey, P. Auger and S. Belliot: *Ultramicroscopy,* 2004, **98**, 219–230.
85. M. Takeda, H. Oka and I. Onaka: *Phys. Status Solidi (a)*, 1992, **132**, 305–322.
86. M. Natan and R. A. Chihoski: *J. Mater. Sci.*, 1983, **18**, 3288–3298.

International Materials Reviews IMR413.3d 22/4/05 21:25:02
The Charlesworth Group, Wakefield +44(0)1924 369598 - Rev 7.51n/W (Jan 20 2003)

S.C. Wang and M.J. Starink, Review of precipitation in Al-Cu-Mg(-Li) alloys, Int Mater Rev., 2005, Vol. 50, pp 193-215

87. M. Takeda, Y. Maeda, A. Yoshida, K. Yauta, S. Konuma and T. Endo: *Scripta Mater.*, 1999, **41**, 643–649.
88. A. Guinier: *J. Phys. Radium*, 1942, **8**, 124–136.
89. V. Gerold: *Z. Metallkde*, 1954, **45**, 599–607.
90. C. Wolverton: *Philos. Mag. Lett.*, 1999, **79**, 683–690.
91. S. Q. Wang, M. Schneider, H. Q. Ye and G. Gottstein: *Scripta Mater.*, 2004, **51**, 665–669.
92. H. Yoshida: *Scripta Metall.*, 1988, **22**, 947–951.
93. T. Sato and T. Takahashi: *Scripta Metall.*, 1988, **22**, 941–946.
94. K. Hirano: *Mater. Sci. Forum*, 1987, **13**, 215.
95. M. Karlik and B. Jouffrey: *Acta Mater.*, 1997, **45**, 3251–3263.
96. I. L. Polmear and H. K. Hardy: *J. Inst. Metals*, 1954, **5**, 393–394.
97. D. A. Porter and K. E. Easterling: 'Phase transformations in metals and alloys', 2nd edn; 1989, Chapman & Hall.
98. L. M. Wang, H. M. Flower and T. C. Lindley: *Scripta Mater.*, 1999, **41**, 391–406.
99. F. Lefebvre, S. C. Wang, M. J. Starink and I. Sinclair: *Mater. Sci. Forum*, 2002, **396–402**, 1555–1560.
100. J. H. Auld: *Acta Crystallogr. Suppl.*, 1972, **28A**, S98.
101. J. H. Auld: *Mater. Sci. Technol.*, 1986, **2**, 784–787.
102. R. J. Chester and I. J. Polmear: in 'The metallurgy of light alloys', 75; 1983, London, Institute of Metals.
103. S. Kerry and V. D. Scott: *Met. Sci.*, 1984, **18**, 289–294.
104. K. M. Knowles and W. M. Stobbs: *Acta Crystallogr.*, 1988, **44B**, 207–227.
105. A. Garg and J. M. Howe: *Acta Metall. Mater.*, 1991, **39**, 1939–1946.
106. R. W. Fonda, W. A. Cassada and G. J. Shiflet: *Acta Metall. Mater.*, 1992, **40**, 2539–2546.
107. J. C. Huang and A. J. Ardell: *Mater. Sci. Technol.*, 1987, **3**, 176–188.
108. L. Reich, M. Murayama and K. Hono: *Acta Mater.*, 1998, **46**, 6053–6062.
109. R. Yoshimura, T. J. Konno, E. Abe and K. Hiraga: *Acta Mater.*, 2003, **51**, 4251–4266.
110. D. Vaughan and J. M. Silcock: *Phys. Status Solidi*, 1967, **20**, 725–736.
111. Y. Jin, C. Z. Li and M. G. Yan: *J. Mater. Sci.*, 1991, **26**, 3244–3248.
112. I. N. A. Oguocha, Y. Jin and S. Yannacopoulos: *Mater. Sci. Technol.*, 1997, **13**, 173–181.
113. S. Abis, P. Mengucci and G. Riontino: *Philos. Mag. B*, 1993, **67**, 465–484.
114. J. A. Taylor, B. A. Parker and I. J. Polmear: *Met. Sci.*, 1978, **12**, 478–482.
115. S. Cousland and G. R. Tate: *J. Appl. Crystallogr.*, 1986, **19**, 174–180.
116. M. S. Lim, K. E. Tibballs and P. L. Rossiter: *Z. Metallkd.*, 1997, **88**, 236–245.
117. A. Garg, Y. C. Chang and J. M. Howe: *Scripta Metall. Mater.*, 1990, **24**, 677–680.
118. K. Hono: *Acta Metall. Mater.*, 1993, **41**, 829–838.
119. B. A. Shollock, C. R. M. Grovenor and K. M. Knowles: *Scripta Metall. Mater.*, 1990, **24**, 1239–1244.
120. C. R. Hutchinson, X. Fan, S. J. Pennycool and G. J. Shiflet: *Acta Mater.*, 2001, **49**, 2827–2841.
121. S. C. Wang, C. Z. Li, Y. L. Wu, J. Qiang and Y. F. Han: *J. Mater. Sci. Lett.*, 1991, **10**, 643–645.
122. A. K. Mukhopadhyay, D. S. Zhou and Q. B. Yang: *Scripta Metall. Mater.*, 1992, **26**, 237–242.
123. M. Audier, C. Janot, M. de Boissieu and B. Dubost: *Philos. Mag.*, 1989, **60**, 437–466.
124. M. D. Ball and H. Lagace: in 'Aluminium–lithium alloys III', Proc. Third Int. Conf. on Aluminium–Lithium, (ed. C. A. Baker, P. J. Gregson, S. J. Harris and C. J. Peel), Inst. of Metals, University of Oxford, July 1985, 555.
125. A. Loiseau and G. Lapasset: *J. de Phys.*, C3, 1986, **47**, 331–340.
126. K. S. Prasad, A. A. Gokhale, A. K. Mukhopadhyay, D. Banerjee and D. B. Goel: *Mater. Sci. Forum*, 2000, **331–337**, 1043–1048.
127. L. C. Zhang, A. Q. He and H. Q. Ye: *Scripta Metall. Mater.*, 1994, **30**, 63–66.
128. S. C. Wang, C. Z. Li and M. G. Yan: *J. Mater. Sci. Lett.*, 1993, **12**, 1178–1181.
129. E. E. Cherkashin, P. I. Kripyakevich and G. I. Oleksiv: *Sov. Phys. Crystallogr.*, 1964, **8**, 681.
130. S. C. Wang, C. Z. Li and M. G. Yan: *J. Mater. Sci. Lett.*, 1993, **12**, 387–389.
131. S. C. Wang, C. Z. Li and M. G. Yan: *J. Mater. Sci.*, 1994, **29**, 384–388.
132. J. M. Silcock: *J. Inst. Met.*, 1959–60, **88**, 357–364.
133. N. Ryum: *Acta Metall.*, 1969, **17**, 269–278.
134. A. K. Vasudevan, E. A. Ludwiczak, S. F. Baumann, P. R. Howell, R. D. Doherty and M. M. Kersker: *Mater. Sci. Technol.*, 1986, **2**, 1205–1209.
135. P. J. Gregson and H. M. Flower: *J. Mater. Sci. Lett.*, 1984, **3**, 829–834.
136. M. J. Starink, P. Wang, I. Sinclair and P. J. Gregson: *Acta Mater.*, 1999, **14**, 3841–3853.
137. H. M. Flower and P. J. Gregson: *Mater. Sci. Technol.*, 1987, **3**, 81–90.
138. B. P. Huang and Z. Q. Zheng: *Acta Metall.*, 1988, **46**, 4381–4393.
139. H. K. Hardy and J. M. Silcock: *J. Inst. Met.*, 1955–56, **84**, 423–428.
140. W. A. Cassada, G. J. Shiflet and E. A. Starke: *J. de Phys.*, C3, 1987, **48**, 397–406.
141. J. M. Howe, J. Lee and A. K. Vasudevan: *Metall. Trans.*, 1988, **19A**, 2911–2920.
142. R. A. Herring, F. W. Gayle and J. R. Pickens: *J. Mater. Sci.*, 1993, **28**, 69–73.
143. K. S. Vecchio and D. B. Williams: *Metall. Trans.*, 1988, **19A**, 2885–2891.
144. S. Van Smaalen, A. Meetsma and J. L. de Boer: *J. Solid State Chem.*, 1990, **85**, 293–298.
145. R. J. Rioja and E. A. Ludwiczak: in 'Aluminium–lithium alloys III', Proc. Third Int. Conf. on Aluminium–Lithium, (ed. C. A. Baker, P. J. Gregson, S. J. Harris and C. J. Peel), Inst. of Metals, University of Oxford, July 1985, 471–479.
146. J. C. Huang and A. J. Ardell: in 'Aluminium–lithium alloys III', Proc. Third Int. Conf. on Aluminium–Lithium, (ed. C. A. Baker, P. J. Gregson, S. J. Harris and C. J. Peel), Inst. of Metals, University of Oxford, July 1985, 455–470.
147. W. A. Cassada, G. J. Shiflet and E. A. Starke: *Scripta Metall.*, 1987, **21**, 387–482.
148. M. H. Tosten and P. R. Howell: in 'Aluminium alloys, their physical and mechanical properties', Proc. Int. Conf. on Aluminium Alloys, (ed. E. A. Starke, Jr and T. H. Sanders, Jr), EMAS, Warley, West Midlands, UK, 1986, 727–741.
149. B. Noble and G. E. Thompson: *Met. Sci. J.*, 1972, **6**, 167–174.